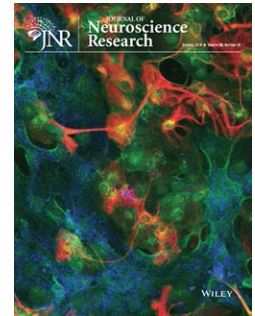



RESEARCH ARTICLE



Synergistic PXT3003 therapy uncouples neuromuscular function from dysmyelination in male Charcot-Marie-Tooth disease type 1A (CMT1A) rats

Thomas Prukop^{1,2}  | Stephanie Wernick^{1,3} | Lydie Boussicault⁴ | David Ewers^{1,3} | Karoline Jäger⁵ | Julia Adam¹ | Lorenz Winter¹ | Susanne Quintes^{1,3} | Lisa Linhoff^{1,3} | Alonso Barrantes-Freer⁶ | Michael Bartl³ | Dirk Czesnik³ | Jana Zschüntzsch⁵ | Jens Schmidt⁵ | Gwenaél Primas⁴ | Julien Laffaire⁴ | Philippe Rinaudo⁴ | Anthony Bureau⁴ | Serguei Nabirovitchkin⁴ | Markus H. Schwab¹ | Klaus-Armin Nave¹ | Rodolphe Hajj⁴ | Daniel Cohen⁴ | Michael W. Sereda^{1,3}

¹Department of Neurogenetics, Max Planck Institute of Experimental Medicine, Göttingen, Germany

²Institute of Clinical Pharmacology, University Medical Center Göttingen, Göttingen, Germany

³Department of Clinical Neurophysiology, University Medical Center Göttingen, Göttingen, Germany

⁴Pharnext, Issy-Les-Moulineaux, France

⁵Department of Neurology, University Medical Center Göttingen, Göttingen, Germany

⁶Department of Neuropathology, University Medical Center Leipzig, Leipzig, Germany

Correspondence

Michael W. Sereda, Research Group "Molecular and Translational Neurology", Department of Neurogenetics, Max-Planck-Institute of Experimental Medicine, Hermann-Rein-Str. 3, D-37075 Göttingen, Germany.

Email: sereda@em.mpg.de

Funding information

This study was funded by Pharnext; MWS held a DFG Heisenberg Professorship (SE 1944/1-1) and was supported by the German

Abstract

Charcot-Marie-Tooth disease 1 A (CMT1A) is caused by an intrachromosomal duplication of the gene encoding for *PMP22* leading to peripheral nerve dysmyelination, axonal loss, and progressive muscle weakness. No therapy is available. PXT3003 is a low-dose combination of baclofen, naltrexone, and sorbitol which has been shown to improve disease symptoms in *Pmp22* transgenic rats, a bona fide model of CMT1A disease. However, the superiority of PXT3003 over its single components or dual combinations have not been tested. Here, we show that in a dorsal root ganglion (DRG) co-culture system derived from transgenic rats, PXT3003 induced myelination when compared to its single and dual components. Applying a clinically relevant ("translational") study design in adult male CMT1A rats for 3 months, PXT3003, but not its dual components, resulted in improved performance in behavioral motor and sensory endpoints when compared to placebo. Unexpectedly, we observed only a marginally increased number of myelinated axons in nerves from PXT3003-treated CMT1A rats. However, in electrophysiology, motor latencies correlated with increased grip strength indicating a possible effect of PXT3003 on neuromuscular junctions (NMJs) and muscle fiber pathology. Indeed, PXT3003-treated CMT1A rats displayed an increased perimeter of individual NMJs and a larger number of functional NMJs. Moreover, muscles of PXT3003 CMT1A rats displayed less neurogenic atrophy and a shift toward fast contracting muscle fibers. We suggest that ameliorated motor

Thomas Prukop and Stephanie Wernick contributed equally to this work.

Edited by Scott Brady. Reviewed by Young Bin Hong and Katherine Halievski.

This is an open access article under the terms of the Creative Commons Attribution-NonCommercial-NoDerivs License, which permits use and distribution in any medium, provided the original work is properly cited, the use is non-commercial and no modifications or adaptations are made.

© 2020 The Authors. Journal of Neuroscience Research published by Wiley Periodicals LLC

Ministry of Education and Research (BMBF, CMT-BIO, FKZ: 01ES0812, CMT-NET, FKZ: 01GM1511C, CMT-NRG, ERA-NET'ERARE3', FKZ: 01GM1605). MWS, TP, and KAN were supported by the European Leukodystrophie Society (ELA 2014-02011). KAN is supported by the DFG (SPP1757 and CNMPB) and holds an ERC Advanced Grant. JZ, JS, and MWS are members of the European Reference Network for Rare Neuromuscular Diseases (ERN EURO-NMD).

function in PXT3003-treated CMT1A rats result from restored NMJ function and muscle innervation, independent from myelination.

KEYWORDS

Charcot-Marie-Tooth, myelination, neuromuscular, PXT3003, RRID:AB_477272, RRID:AB_1157897, RRID:AB_1556321, RRID:AB_2564642, RRID:AB_2147165, RRID:AB_2266724, RRID:AB_10572253, RRID:AB_10746275, therapy

1 | INTRODUCTION

Charcot-Marie-Tooth disease (CMT) is a heterogeneous group of hereditary neuropathies (Brennan, Bai, & Shy, 2015). The population prevalence is estimated to approximately 1 in 2,500 caused by more than 100 gene mutations known to date (Pipis, Rossor, Laura, & Reilly, 2019; Rossor, Tomaselli, & Reilly, 2016). Genetic defects affect either primarily the Schwann cell leading to dys- or demyelination followed by axonal loss, or first impair neuronal function, including axonal integrity, followed by myelination defects (Rossor, Evans, & Reilly, 2015). Eventually, slowly progressive and predominantly motor symptoms like muscle weakness are observed. The most common CMT form (CMT1A) is caused by an intrachromosomal duplication of the gene encoding for the "peripheral myelin protein of 22KD (PMP22)" (Lupski et al., 1991; Lupski & Garcia, 1992; Raeymaekers et al., 1991), a small myelin protein of unknown function (Li, Parker, Martyn, Natarajan, & Guo, 2013). Fifty percent overexpression of PMP22 causes peripheral nerve dysmyelination, axonal dysfunction, and loss and progressive muscle weakness in patients which can be well modeled in a *Pmp22* transgenic rat model ("CMT1A rat") (Fledrich et al., 2014, 2018, 2019a, 2019b; Murphy et al., 2012; Rossor et al., 2015, 2016; Sereda et al., 1996).

Currently, there is no approved drug therapy available for CMT patients. Preclinical studies in CMT rats focused on the reduction of *Pmp22* mRNA overexpression by targeting the progesterone receptor (Meyer zu Horste et al., 2007) or the P2X7 calcium purinoceptor (Sociali et al., 2016) which led to phenotype amelioration. More recently, antisense oligonucleotides were also shown effective in reducing *Pmp22* mRNA overexpression in CMT1A rats (Zhao et al., 2018). Thus, transcriptional *Pmp22* regulation is a relevant target for therapeutic trials in CMT1A patients. Other strategies independent of targeting *Pmp22* were also proven effective on disease progression as well, for example, lipid supplementation (Fledrich et al., 2018). However, these approaches were either not suitable for clinical trials (Fledrich et al., 2014; Meyer zu Horste et al., 2007), failed in clinical testing (Lewis et al., 2013; Pareyson et al., 2011) or have not been translated into patients yet (Fledrich et al., 2018; Sociali et al., 2016; Zhao et al., 2018).

PXT3003 is a fixed-ratio combination of baclofen (BCL), naltrexone (NTX), and sorbitol (SRB) and is currently the most developed drug for CMT1A patients. Using a systems biology approach, these three single components were predicted to lower *Pmp22* mRNA

Significance

We describe an improvement of muscle and sensory function in adult CMT1A rats treated chronically with PXT3003, a low-dose combination of baclofen, naltrexone, and sorbitol. Importantly, we demonstrate a superior efficacy of PXT3003 when compared to its components, which emphasizes the therapeutic value of combining repurposed drugs at low and safe doses. The function of neuromuscular junctions (NMJ) plays a decisive role in the development of motor strength uncoupled from the degree of peripheral nerve myelination. Therefore, the NMJ may constitute a new pharmacological target for the treatment of CMT1A patients.

expression and improve signaling pathways important for peripheral nerve myelination and axonal function. As a potent agonist of GABA-B receptors, baclofen is described to negatively regulate the transcription of *PMP22* gene in Schwann cells (Magnaghi et al., 2004, 2006). Naltrexone potentiates canonical opioid receptors signaling by activation of $G_{\alpha i}$ proteins and thus may decrease the level of expression of *PMP22* through a mechanism complementing and potentiating baclofen's mechanism of action (Crain & Shen, 2001; Hytrek, McLaughlin, Lang, & Zagon, 1996; Paquette, Olmstead, & Olmstead, 2005; Wang & Burns, 2009; Wang, Frankfurt, & Burns, 2008). Sorbitol may act as a protein chaperone. Indeed, sorbitol has been recently reported to inhibit protein fibrillation and stabilize misfolded polypeptides (Choudhary, Save, Kishore, & Hosur, 2016; Roy & Bhat, 2018). Interestingly, it has been postulated that the decreased yield of properly folded PMP22 at the cell membrane may be a driver for CMT1A characteristic dysmyelination (Mittendorf et al., 2017; Schlebach et al., 2015).

Due to an anticipated synergistic action, the dosages of each single component of PXT3003 were lower than those used for each component in its primary indication. Indeed, a first preclinical study in CMT1A rats confirmed PXT3003 effects on *Pmp22* mRNA expression, myelination and axonal loss leading to an improved motor and sensory functions (Chumakov et al., 2014). The effect was even more striking after early postnatal short-term administration of PXT3003 which lowered *Pmp22* overexpression, improved axonal

diameter distribution, and partially prevented phenotypic disease manifestation in CMT1A rats (Prukop et al., 2019). To translate these preclinical findings to patients, clinical trials were initiated. Clinical effectiveness was demonstrated in an exploratory phase 2 study in CMT1A patients (Attarian et al., 2014, 2016) and was tested in an international phase 3 clinical study (Vita et al., 2019). However, to which extent the global effect of PXT3003 depends on its individual components remains elusive.

Beyond established axonal and myelin deficits in CMT1A pathology, the impact of abnormal synaptic transmission at the neuromuscular junction (NMJ) has not been investigated in detail in preclinical trials. Structural and functional alterations of the NMJ are frequently present in affected nerves, but their contribution to impaired motor function remains unclear (Nicks et al., 2013). Previous investigations identified a reduced number of functional NMJs in a *Pmp22* transgenic mouse model of CMT1A (Ang et al., 2010; Shi, Fu, & Ip, 2012). In addition, synaptic dysfunction was shown to be a cause of muscle weakness and fatigue in a mouse model of CMT2D (Spaulding et al., 2016). Impaired synaptic transmission and the number and functionality of NMJs is thought to contribute to disease severity and progression in the *Trembler-J* mouse, a model of CMT1E carrying a mutation in the *Pmp22* gene (Scurry et al., 2016).

Because the original strain of the CMT1A rats (Sereda et al., 1996) which were kept as outbred strains may have lost transgene copies after multiple generations, we revitalized the original strain of CMT1A rats from frozen embryos and used these in the present *in vivo* investigations, in contrast to the formerly described preclinical study of PXT3003 in adult and young CMT1A rats (Chumakov et al., 2014; Prukop et al., 2019). Thus, we first re-evaluated behavioral endpoints including the optimal effective PXT3003 dose, but retaining the same fixed ratio used formerly in CMT1A rats (Chumakov et al., 2014; Prukop et al., 2019) and phase 2 and 3 clinical trials in CMT1A patients (Attarian et al., 2014, 2016; Vita et al., 2019).

Second, we performed a detailed investigation into synergistic effects of PXT3003 in comparison to its single components BCL, NTX, and SRB using a DRG co-culture system. We then performed a translational, clinically relevant *in vivo* study in which CMT1A rats were treated with PXT3003 or one of its dual components for 3 months including phenotyping and electrophysiology. In order to examine effects of PXT3003 treatment on the motor unit in CMT1A rats, analyses were extended to the peripheral nerve, the NMJs and muscles.

2 | MATERIALS AND METHODS

2.1 | Ethics

The *in vivo* studies was reviewed by an in-house review committee at the Max Planck Institute of Experimental Medicine, and approved by the Niedersächsisches Landesamt für Verbraucherschutz und Lebensmittelsicherheit (LAVES) (Approval number:

33.19-42502-04-16/2200). The *in vitro* study was conducted in accordance with the National Institutes of Health Guide for the Care and Use of Laboratory Animals and followed current European Union regulations Directive 2010/63/UE (Agreement number: A1301310).

2.2 | *Pmp22* transgenic rats

We used revitalized male *Pmp22* transgenic Sprague–Dawley rats containing the complete murine *Pmp22* gene including 7 kb upstream of exon 1A and 4 kb downstream of exon 5 and leading to approx. 1.6-fold *Pmp22* mRNA overexpression (Sereda et al., 1996), called CMT1A rats, including male wildtype littermates as controls. Rats were outbred (Max Planck Institute of Experimental Medicine, Göttingen, Germany) and had free access to water and sorbitol-free food (V1325-318, SNIFF). Genotyping was performed as recently described (Fledrich et al., 2018).

2.3 | DRG co-culture system derived from *Pmp22* transgenic (CMT1A) rats

Male *Pmp22* transgenic Sprague–Dawley rats were bred with WT Sprague–Dawley females (Janvier Labs, France). To determine *Pmp22* genotype of embryos, DNA was extracted from a piece of embryo head using the SYBR Green Extract-N-Amp tissue PCR kit and a qPCR was performed using the SYBR Green Master Mix kit (Sigma Aldrich, cat#XNATG-1KT). *Pmp22* gene was determined using mouse-specific *Pmp22* primers (forward: 5'-GACAAACCCAGACAGTTG-3' and reverse: 5'-CCAGAAAGCCAGGGAAGCT-3'). Genotyping, co-cultures and immunostaining were performed at NeuroSys (Gardanne, France). Sex of the embryo was not genotyped; male and female embryos were included in co-cultures.

Pmp22 transgenic and WT sensory neurons were cultured as previously described (Callizot, Combes, Steinschneider, & Poindron, 2011). Briefly, the dorsal root ganglia (DRG) from 15-day-old embryos were collected and treated with trypsin 0.25%-EDTA 0.02% (Pan Biotech, cat#P10-023100). The reaction was stopped by adding DMEM containing 10% of fetal bovine serum in the presence of DNase I grade II (final concentration 0.5 mg/ml; Pan Biotech P60-37780100). The suspension was mechanically dissociated and then centrifuged at 350× g for 10 min. Pellet was re-suspended in neurobasal medium (Invitrogen, cat# 11570556) supplemented with B27 (2%, Invitrogen, cat# 11530536), L-Glutamine (2 mmol/L, PAN Biotech, cat#P04-80100), Penicillin (10.000 U/ml), Streptomycin (10 mg/ml, 2%, Pan Biotech, cat#P06-07100), and Nerve Growth Factor (50 ng/ml, Sigma Aldrich, cat#N1408). Cells were seeded in plates treated with poly-L-lysine (Falcon, cat#356516) and coated with L-laminin (Sigma Aldrich, cat#P2606). After 7 days, ascorbic acid (50 µg/ml, AA), Sigma Aldrich, cat#A92902), single drugs, duos, or PXT3003 were added in culture media. (RS)-baclofen (BCL, 12.8 pM to 200 nM, cat#B5399), Naltrexone hydrochloride (NTX, 0.044 pM to 8 nM, cat#N3136), and D-Sorbitol (SRB, 5.7 pM to

40 nM, cat#S3889) were provided by Sigma Aldrich. Each single drug was first solubilized in sterile water to constitute concentrated stock solutions, which were subsequently filtered and stored at -20°C . Drugs were mixed to constitute PXT3003 (BCL (717 pM) + NTX (0.1 pM) + SRB (320 pM)) or associated duos immediately before addition into the well. Half of the medium was renewed every other day. Co-cultures were maintained at 37°C in a humidified incubator, in an atmosphere of air (95%)-CO₂ (5%).

2.4 | Immunostaining and quantification of myelination in DRG co-cultures

After 35 days of culture (D28 post AA), cells were fixed by a cool solution of ethanol (95%) and acetic acid (5%) for 5 min. After permeabilization with 0.1% of saponin, cells were blocked with PBS containing 10% FBS and incubated with primary antibodies anti-PMP22, (1/50, Sigma Aldrich, cat#SAB4502217, RRID:AB_10746275), anti-MBP (1/1000, Novus Biologicals, cat#NBP1-05204, RRID:AB_1556321), and anti-Neurofilament 200 (1/500, Sigma Aldrich, cat#N4142, RRID:AB_477272) (Table 1). Primary antibodies were revealed with Alexa Fluor 568 goat anti-rabbit IgG (1/400, Sigma Aldrich, cat#SAB4600084). Nuclei were counterstained with the fluorescent dye Hoechst (1/1000, Sigma Aldrich). Immunostaining and pictures were automatically performed by a robotic platform (Beckman Coulter). Thirty pictures per well were taken using ImageXpress (camera CMOS detector, Molecular Devices) at 20 \times magnification. Picture analysis was automatically performed using Custom Module Editor (Molecular Device). Cumulative mean length in micrometer of PMP22, MBP, and Neurofilament were quantified.

2.5 | Transcriptional analysis of RT-qPCR in DRG co-cultures

RT-qPCR analysis of *in vitro* experiments was performed at Pharnext (Evry, France). After 35 days of cultures (D28 post AA), cell cultures were lysed in Qiazol (Qiagen, cat#1023537) and mechanically homogenized with Precellys Evolution device (8 \times 10 s at 8,000 rpm on ice, Bertin). Total RNA was isolated using miRNeasy Micro Kit (Qiagen, cat#1071023) according to the manufacturer's protocol. RNA concentration was quantified using an ND-100 spectrophotometer (Nanodrop Technologies). mRNA was reverse transcribed from 80ng of total RNA using SuperScriptTM II Reverse Transcriptase (ThermoFisher Scientific, cat#18064014). Real-time qPCR was performed using a SYBR green-based detection system (LightCycler 480 SYBR Green I Master (Roche)). *Pmp22* primers recognized both mouse and rat *Pmp22* (forward: 5'-TGTACCACATCCGCCTTGG-3', reverse: 5'-GAGCTGGCAGAAGAACAGGAAC-3'). *Rps9* (forward: 5'-AGCTG GGTTCGTCGCAAAA-3', reverse: 5'-CCTCACGTTTGTTCGGAG-3') expression was used to normalize samples expression.

2.6 | Drugs and dosing in CMT1A rats

PXT3003 is a fixed-ratio mix of RS-baclofen (BCL), naltrexone hydrochloride (NTX), and D-sorbitol (SRB). Compounds were purchased from Sigma and dissolved in phosphate buffer at pH = 5.4 and stored between $+2^{\circ}\text{C}$ and $+8^{\circ}\text{C}$ protected from light for the maximum of 1 week. PXT3003 was dosed in four increasing dosages, called PXT3003-1 (BCL 15 $\mu\text{g}/\text{kg}$ + NTX 1.75 $\mu\text{g}/\text{kg}$ + SRB 0.525 mg/kg), PXT3003-2 (BCL 30 $\mu\text{g}/\text{kg}$ + NTX 3.5 $\mu\text{g}/\text{kg}$ + SRB 1.05 mg/kg), PXT3003-3 (BCL 60 $\mu\text{g}/$

TABLE 1 Listing of primary antibodies

Name	Immunogen	Details	Concentration
Anti-PMP22 antibody produced in rabbit	Anti-PMP22, C-Terminal	Sigma Aldrich, # SAB4502217, rabbit, polyclonal, RRID:AB_10746275	1/50
Anti-Neurofilament 200 antibody produced in rabbit	Neurofilament 200 from bovine spinal cord	Sigma Aldrich, # N4142, rabbit, polyclonal, RRID:AB_477272	1/500
Myelin basic antibody	Purified MBP isolated from bovine brain	Novus Biologicals, #NBP1-05204, mouse, monoclonal, RRID:AB_1556321	1/1000
Purified anti-Neurofilament H (NF-H), Nonphosphorylated Antibody	Neurofilament heavy polypeptide, NF-H, 200 kD	BioLegend, # 801701, batch # B224830, mouse, monoclonal, RRID:AB_2564642	1/500
Myosin heavy chain (slow, alpha-, and beta-) antibody	Myosin heavy chain (slow, alpha-, and beta-)	Developmental Studies Hybridoma Bank, University of Iowa, # BA-F8, mouse, monoclonal, RRID:AB_10572253	1/25
Myosin Heavy Chain Type IIA antibody	Myosin Heavy Chain Type IIA	Developmental Studies Hybridoma Bank, University of Iowa, # SC-71, mouse, monoclonal, RRID:AB_2147165	1/300
Myosin heavy chain, fast, 2X antibody	Myosin heavy chain, fast, 2X	Developmental Studies Hybridoma Bank, University of Iowa, # 6H1, mouse, monoclonal, RRID:AB_1157897	1/50
Myosin Heavy Chain Type IIB antibody	Myosin Heavy Chain Type IIB	Developmental Studies Hybridoma Bank, University of Iowa, # BF-F3, mouse, monoclonal, RRID:AB_2266724	1/15

kg + NTX 7 µg/kg + SRB 2.1 mg/kg), and PXT3003-4 (BCL 180 µg/kg + NTX 21 µg/kg + SRB 6.3 mg/kg). Dual combinations were administered in corresponding dosages to PXT3003-3, called BCL/NTX-3 (BCL 60 µg/kg + NTX 7 µg/kg), BCL/SRB-3 (BCL 60 µg/kg + SRB 2.1 mg/kg), and NTX/SRB-3 (NTX 7 µg/kg + SRB 2.1 mg/kg). Phosphate buffer served as placebo. All animal experiments were performed at the Max-Planck Institute of Experimental Medicine (Göttingen, Germany).

2.7 | In vivo study design

Four weeks aged rats were stratified to ensure balanced distribution between groups based on motor function (grip strength and inclined plane) as well as on age and lineage. Treatment started in adult 6 weeks old male rats and was continued for 12 consecutive weeks by once daily oral gavage. Phenotype was monitored in 6, 10, 14 and 18 weeks old rats (corresponding to baseline, 4, 8, and 12 weeks of treatment) by one investigator blinded toward the treatment. At study end, rats were anaesthetized by a mixture of ketamine hydrochloride (100 mg/kg body weight) and xylazine hydrochloride (8 mg/kg body weight) for electrophysiological measures, followed by overdose of corresponding ketamine hydrochloride/xylazine hydrochloride mixture for euthanasia and tissue collection.

2.8 | Monitoring of motor and sensory phenotype

Grip strength was measured at the hind limbs by supporting the forelimbs and pulling the animal's tail toward a horizontal bar (width 14 cm, diameter 3.2 mm) which was connected to a digital force gauge. The investigator pulled rats horizontally until they lost their grip. The maximum force exerted onto the T-bar was recorded. Measurements were repeated five times, and means were used for analysis. For inclined plane behavior, rats were placed on the 25°-angled inclined plexiglass plane (30 cm × 50 cm) in the up-headed position. Performance was scored as no slide = 0, sliding of one or two paws = 1, sliding of all four paws = 2, or sliding to the very bottom of the plane = 3. For bar holding performance, rats were placed by hand onto a horizontal bar (length 70 cm) and holding time was recorded until rats fall for a maximum of 180 s. The bar diameter was adjusted with increasing age (2.5 cm at 6 weeks, 3.5 at 10 weeks, and 4.0 cm at 14 and 18 weeks). Measurements were repeated three times each, and means were used for analysis. For hot plate reactivity, rats were placed on a 52°C heated plate (25.4 cm × 25.4 cm) surrounded by a clear acrylic cage (30 cm high, open top) (Columbus). The latency to respond either with a hindpaw lick, hindpaw flick, or jump was recorded. Observation time was limited to maximum 60 s. The assessment was only performed once at study end.

2.9 | Electrophysiological analyses of peripheral nerves

We analyzed motor latencies, nerve conduction velocities (NCV), and compound muscle action potentials (CMAP) after stimulation in the

tail and sciatic nerve, each performed once per animal at study end. In the tail, a pair of steel needle electrodes (Schuler Medizintechnik) was placed subcutaneously into the proximal part to the tail (proximal stimulation). A second pair of electrodes was placed 5 cm distally. In the sciatic nerve measurements, needle electrodes were inserted alongside the nerves at the sciatic notch (proximal stimulation) and the hock (distal stimulation). Stimulation was performed with increasing voltage of 0.1 ms duration until supramaximal stimulation (Toennis 3 Neuroscreen®, Jäger or Evidence 3102evo®, Neurosoft). Motor latencies were measured as time interval between stimulation and observed response (for both, proximal and distal stimulation). Nerve conduction velocity was calculated as the ratio of the distance between proximal and distal stimulation and its corresponding latency. Maximum CMAP was calculated peak to peak between negative and positive amplitudes (for both, proximal and distal stimulation).

2.10 | Histological analysis of peripheral nerves

Nerve pathology was investigated in peripheral nerves by axonal counting, axon caliber size, myelin sheath thickness, and internodal length on light microscopic level. Femoral nerves were fixed in 4% paraformaldehyde and 2.5% glutaraldehyde in phosphate buffer, then embedded in epoxy resin and 0.5 µm thick cross sections stained with methylene blue/Azur II, and separately by silver impregnation according to Gallyas. Axon number was quantified in whole nerves cross sections stained with methylene blue/Azur II. Myelin sheath thickness (g-ratio = axon circumference divided by circumference of the axon plus myelin sheath) and axon diameters were analyzed in 200 randomly chosen axons per nerve stained by silver impregnation according to Gallyas. For internodal length analyses, we fixed freshly prepared tibial nerves in 4% paraformaldehyde for 30 min and transferred them to phosphate buffered saline to pull out bundles of axons. Up to 10 slides per animal of longitudinally isolated axons were stained with osmium to visualize nodal structures, then the distance between each two nodes was measured and means calculated per each animal for analysis.

2.11 | Histological analysis of neuromuscular junctions (NMJ)

We used freshly frozen 35 µm thick longitudinal sections of the gastrocnemius muscle. Motor endplates were visualized by cholinesterase staining via incubation with buffered 5-bromoindoxyl acetate for 45 min at 37°C (Pestronk & Drachman, 1978). Second, after blocking with 4% horse serum, freshly frozen cross sections were incubated with neurofilament H (NF-H) 200 kDa (1:500, BioLegend, No. 801701, RRID:AB_2564642) primary antibody at 4°C overnight (Table 1), followed by visualization of presynaptic fibers and terminals using Cy3-conjugated IgG secondary antibody. Postsynapses were stained with Alexa Fluor 488-conjugated α-bungarotoxin (1:500, Molecular Probes Eugene).

2.12 | Histological analysis of the muscle

For morphologic analyses of atrophic angular fibers in CMT1A rats, 10- μ m cross sections of gastrocnemius muscle were cut on a cryomicrotome (CM 3050 S; Leica Microsystems) and stained with hematoxylin and eosin (H&E; Mayer's hematoxylin and eosin; Merck). The sections were mounted with Entellan (Merck). The number of normal muscle fibers was counted in comparison to the number of angular configured muscle fibers in up to three different areas of the tissue section. For muscle fiber subtyping analysis (myosin heavy chain; MHC expression) 10- μ m cross sections of gastrocnemius muscle were air dried and fixed with Acetone (Carl Roth) for 20 min. Sections were blocked with PBS containing 10% NGS (Merck) and incubated with primary antibodies against MHCI (BA-F8, 1/25, mouse IgG2b, RRID:AB_10572253), MHCIIa (SC-71, 1/300, mouse IgG1, RRID:AB_2147165), MHCIIx (6H1, 1/50, mouse IgM, RRID:AB_1157897), MHCIIb (BF-F3, 1/15, mouse IgM, RRID:AB_2266724) (all from the Developmental Studies Hybridoma Bank, University of Iowa) (Table 1). Primary antibodies were revealed with the corresponding goat anti-mouse antibody at a concentration of 1/500 (Alexa Fluor 350 IgG2b, Alexa Fluor 488 IgG1) or 1/250 (Alexa Fluor 594 IgM) (all from Invitrogen). The sections were mounted with Fluoromount G (Southern Biotech).

2.13 | Transcriptional analyses of peripheral nerves

Freshly frozen sciatic nerves were homogenized in 80% sucrose buffer containing protease and phosphatase inhibitors according to manufacturer's instructions (Roche). First, lysates were added to RLT buffer and RNA isolation (Qiagen) including cDNA syntheses following manufacturer's instructions (ThermoFischer). SYBR Green® (Qiagen) quantitative reverse transcriptase PCR (RT-PCR) followed a two-step protocol (LC480, Roche) and quantitation of PCR product was performed using the comparative $\Delta\Delta C_t$ method. Each sample was measured in three replicates and averaged for analyses. For quantification of gene expression, the amplification was normalized against the mean of the two most stable reference genes. The primer sequences were as follows: *Pmp22* fwd TGTACCACATCCGCCTTGG and rev GAGCTGGCAGAAGAACAGGAAC, *Jun* fwd CCTTCTACGACGATGCCCTC and rev GGTTCAGGTCATGCTCTGTTT, *Sox2* fwd TCCAAAACTAATCACAAACATCG and rev GAAGTGCAAT TGGGATGAAAA, *Lpl* fwd TCCTACTTCCGCTGGTCAGA and rev CCTGGCAGAGAAGATGACCT, *Igf1* fwd TGTAACGACCCGGGACG and rev GAGATGTGAAGACGACATGATGTG, *Hprt1* fwd GGTCCATTCTATGACTGTAGATTTT and rev CAATCAAGACGTTCTTTCCAGTT, *Gapdh* fwd AGGAACACGGAAGGCCATG and rev ATGCCCTCTGGAAAGCT, *Rplp0* fwd GATGCCAGGGAAGACAG and rev CACAATGAAGCATTTGGGTAG, *Rps18* fwd AAATCAGTTATGGTTCCTTTGGTC and rev GCTCTAGAATTACCACAGTTATCCAA.

2.14 | Transcriptional analyses of muscle

Frozen tissue from gastrocnemius muscles was homogenized in 350 μ l Trizol reagent (Qiagen) in an electric homogenizer (Precellys 24, Peqlab). RNA was isolated using the RNA Easy kit (Qiagen), following the manufacturer's instructions. Two hundred nanograms of RNA was converted to double-stranded cDNA using SuperScript (Invitrogen) according to the manufacturer's protocol. Relative mRNA levels were quantified with quantitative (real-time, RT) PCR using fluorescent TaqMan technology (Thermo Fisher Scientific). PCR primer and probe specific for rat MHCIIb were obtained as TaqMan predeveloped assay reagents for gene expression from Thermo Fisher Scientific (assay IDs: MHCI: Rn01488777_g1, MHCIIa: Rn01470656_m1, MHCIIb: Rn01496087_g1, MHCIIx: Rn01751056_m1). In a 20- μ l reaction, 0.5 μ l cDNA was amplified using the real-time PCR cyclers ABI 7900 (Applied Biosystems). Glyceraldehyde 3-phosphate dehydrogenase (*Gapdh*, assay ID: Rn01462662_g1, Thermo Fisher Scientific) was used as endogenous control to quantify the relative amount of sample DNA according to the $2^{-\Delta\Delta C_t}$ method.

2.15 | Statistical considerations

The main objectives of the first *in vivo* study (dose finding) were explorative to characterize the revitalized CMT1A rat model, define the optimal dose of PXT3003 on motor and sensory behavior including other exploratory effects of PXT3003 on electrophysiological parameters, transcriptional markers, axons, myelin, and neuromuscular junctions. The main objectives of the second *in vivo* study were to confirm PXT3003 efficacy in CMT1A rats on motor and sensory behavior, to compare the superiority of PXT3003 against its duos on the same endpoints and to explore other effects of PXT3003 on electrophysiological parameters, transcriptional markers, axons, and myelin.

The number of animals used in the studies was defined by a-priori power analysis taking own experience with the CMT1A rat model into consideration aiming at the demonstration of significant grip strength effects (Fledrich et al., 2012, 2014; Meyer zu Horste et al., 2007; Prukop et al., 2019; Sereda, Meyer zu Hörste, Suter, Uzma, & Nave, 2003; Sociali et al., 2016).

We used GraphPad Prism software for statistical analysis. For *in vitro* data and hot plate test (performed once at study end), significance was determined by applying an ANOVA and a Dunnett's multiple comparison test for comparison of more than two groups. For behavioral motor data (grip, bar and inclined plane), a two-way ANOVA with a Dunnett's test was applied on the raw data transformed as change from baseline. An unpaired Student's *t* test was additionally used as supportive technique on raw data for trend assessments. Analysis of exploratory histological and molecular data was performed with a *t* test. Statistical tests were two-tailed and conducted at a 5% significance level.

In vitro synergy was assessed using the Response Additivity (RA) model, an effect-based approach of drug combination analysis (Foucquier & Guedj, 2015). It was used to compare the observed combination effect of PXT3003 to the expected addition effect of its single and duo components. This analysis was performed using Pharnext internal R package pxt.synergy.v1 on R system version 3.6.0.

Full data sets were used for in-life analysis. Exploratory post-mortem analyses were performed in data subsets. Animals were then randomly chosen, and the number increased in the case of high variability masking putative effects.

Group sizes are mentioned, and significance as $p < 0.05$ is indicated in the figures, and symbols used (#, * and +) are explained in the

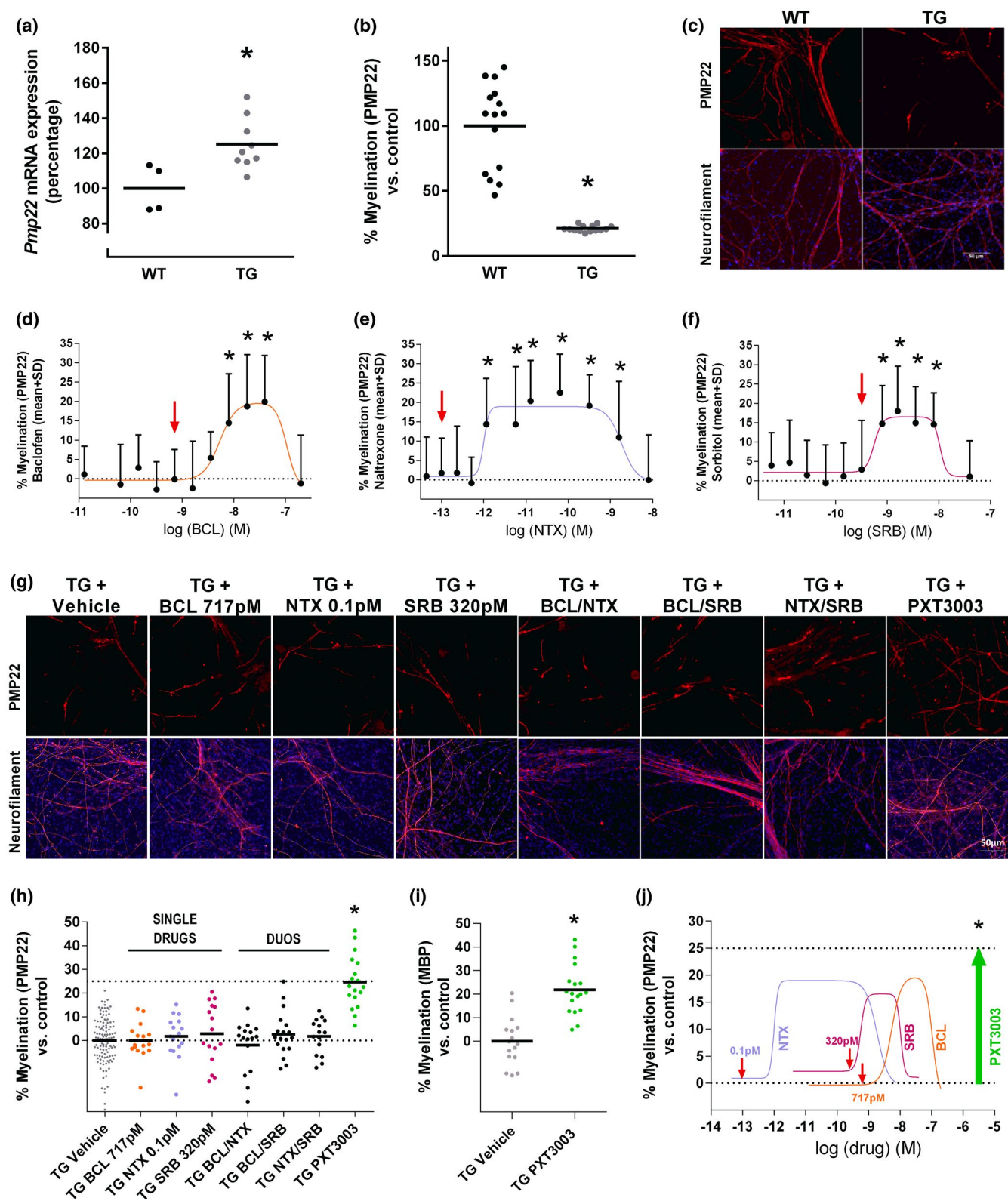


FIGURE 1 Superior *in vitro* activity of PXT3003 on myelination compared to its components. Transgenic DRG co-culture system derived from *Pmp22* transgenic rats (CMT1A) was characterized by an overexpression of *Pmp22* (a) and decreased myelin around axons (b) as quantified and illustrated for PMP22 and neurofilament staining (c). Dose-response curves are shown for Baclofen (BCL) (d), Naltrexone (NTX) (e), and Sorbitol (SRB) on myelination (f). PXT3003 increased myelination compared to its single drugs and dual combinations at the corresponding concentrations when stained for PMP22 (g,h); and PXT3003 effect was independently confirmed when stained for MBP (i). Sub-active concentrations of single drugs BCL, NTX, and SRB exert a synergistic action when combined in PXT3003; red arrows indicate the chosen sub-active concentrations of single drugs (d–f, j). In (a), $n = 1$ culture and 4 replicates for WT, and $n = 3$ independent cultures and 3 replicates per culture for TG (total of 9 replicates for TG); in (b–j), $n = 3$ independent cultures with 5–6 replicates per culture (total of 15–18 replicates). h: as conditions were performed on different plates, all vehicles from different plates were merged explaining the high number of measures for the vehicle control condition. * $p < 0.05$ for comparison to non-treated WT (a,b), or to vehicle transgenic (c–j); dot plots and means, otherwise means and SD (d–f). ANOVA one way + Dunnett: (d): $F(11, 195) = 10.90$, $p < 0.0001$, (e): $F(11,197) = 12.08$, $p < 0.0001$, (f): $F(11, 202) = 7.797$, $p < 0.0001$ and (h): $F(7,222) = 14.83$, $p < 0.0001$

corresponding legends. Data are presented as dot plots and means, or as means and standard deviation (SD) as indicated in the legends.

3 | RESULTS

3.1 | Superior *in vitro* activity of PXT3003 on myelination compared to its components

We used a DRG sensory neuron/Schwann cell co-culture system derived from *Pmp22* transgenic (CMT1A) rats to investigate PXT3003 activity on myelination and related signaling pathways compared to single and dual components.

We observed a $125.2 \pm 14.62\%$ significant overexpression of *Pmp22* mRNA (Figure 1a) and a significantly decreased myelination of axons in the transgenic system ($21.2 \pm 2.4\%$) (Figure 1b,c) when stained for PMP22 and compared to wildtype ($100.0 \pm 13.4\%$ and $100.0 \pm 33.4\%$, respectively).

Co-cultures were treated after Schwann cell proliferation starting at 7 days *in vitro* for 28 days. Dose-response curves were generated for single BCL (Figure 1d), NTX (Figure 1e), and SRB (Figure 1f) on myelination to describe their activity individually and to selected sub-active doses for synergy assessment. When components were combined at sub-active concentrations into PXT3003, the combination significantly increased myelination by $24.6 \pm 11.0\%$ when stained for PMP22 compared to untreated transgenic co-cultures, while single drugs and dual combinations were not significantly effective at the corresponding concentrations on myelination (Figure 1g,h). A control experiment confirmed increased myelination for PXT3003 when stained for another myelin marker MBP, and when compared to untreated transgenic controls (Figure 1i). Figure 1j summarizes the synergistic action and superiority of PXT3003 on PMP22, which exceeds the maximum effects of its single drugs.

3.2 | Superior behavioral performance of PXT3003 compared to dual combinations in CMT1A rats

We performed two separate studies starting in affected 6 weeks aged male CMT1A rats following chronic dosing for 3 months. In the first study, PXT3003 was applied at four increasing dosages to male CMT1A rats, each $n = 19$ –20 per group (called PXT3003-1,

PXT3003-2, PXT3003-3, and PXT3003-4). In the second study, PXT3003-3 and its corresponding dual combinations were applied to male CMT1A rats, each $n = 19$ –20 per group (called BCL/NTX-3, BCL/SRB-3, and NTX/SRB-3). Both studies were placebo controlled for male CMT1A and wildtype rats, each $n = 20$ –21 per group. Prior to the start of the treatment, 4 weeks aged rats were assessed by a subset of behavioral measures to ensure balanced stratification between groups.

At stratification, all CMT1A groups showed decreased grip strength at the hindlimbs and increased deficit score in the inclined plane test compared to wildtype (WT) placebo, and importantly, these deficits were equally balanced between all CMT1A groups (Figures S1a,b and S2a,b). At treatment start (baseline, 6 weeks of age), we observed few variations between CMT1A groups in the behavioral tests. Therefore, data were presented both as raw and as change from baseline.

In the first study, continuous grip strength measurements revealed a muscle weakness in CMT1A placebo rats throughout the entire study period compared to WT placebo, reaching 5.6 ± 1.1 N compared to 8.7 ± 0.7 N at study end (Figure 2a). PXT3003-treated CMT1A rats continuously gained muscle strength until study end to 6.6 ± 1.5 N for PXT3003-1, 6.7 ± 1.2 N for PXT3003-3, and 6.9 ± 1.8 N for PXT3003-4 (Figure 2a and Figure S1c). Analysis of the change from baseline shows the significant therapy effects for PXT3003-3 and PXT3003-4 groups at study end (Figure 2b).

The bar holding test showed deficits in CMT1A placebo rats compared to WT placebo throughout the entire study period. At study end, CMT1A placebo showed lower bar holding time of 11.9 ± 11.7 s compared to 180.0 ± 0.0 s in WT placebo (Figure 2c). PXT3003-treated CMT1A rats continuously improved their holding performance resulting in an increased bar holding time of 33.3 ± 44.0 s for PXT3003-2 and 36.0 ± 40.8 s for PXT3003-3 when compared to CMT1A placebo (Figure 2c,d). Analysis of the change from baseline revealed the highest improvement for PXT3003-3 group at study end by trend (Figure S1d).

The inclined plane behavior also revealed significantly higher deficit scores in CMT1A placebo rats compared to WT placebo, but we observed a high variability in this model as well as decreasing differences between CMT1A placebo and WT placebo rats over time, which limited the relevance of this test for long-term monitoring aims (Figure S1e). Nevertheless, of note, at study end CMT1A placebo still showed higher deficit scores of 0.29 ± 0.49 compared to 0.0 ± 0.0 in

WT placebo whereas PXT3003-3 treated CMT1A rats corrected the deficit score to 0.0 ± 0.0 (Figure S1f), but the analysis of the change from baseline did not show any therapy effects (Figure S1g).

Finally, a sensory endpoint was assessed at study end. CMT1A placebo rats showed significantly delayed thermal reactivity time in the hot plate test of 13.6 ± 1.6 s compared to 7.2 ± 0.8 s in WT

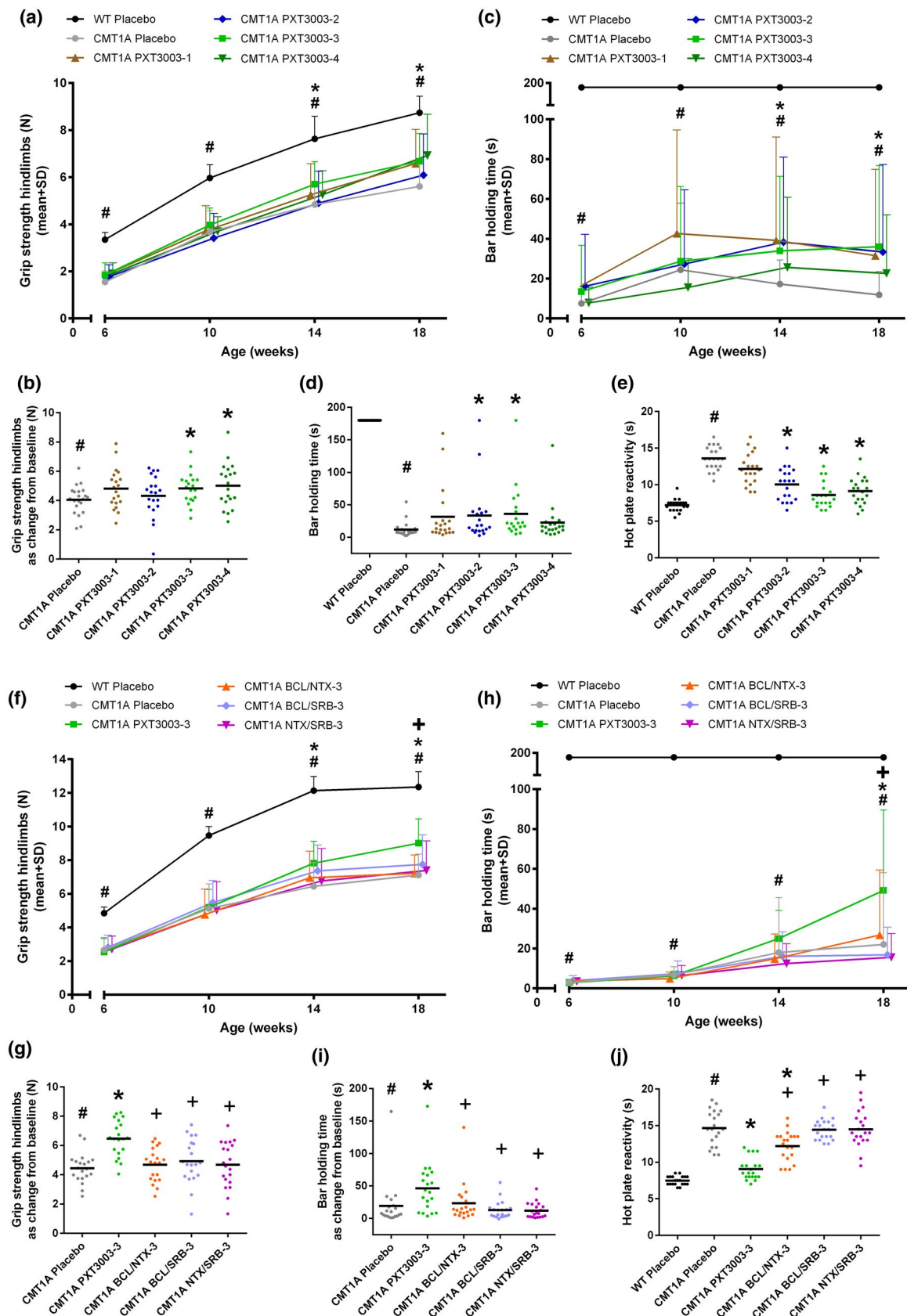


FIGURE 2 Superior behavioral performance of PXT3003 compared to its dual combinations in CMT1A rats. Two separate treatment regimens were applied: the first with four increasing PXT3003 dosages, and the second with the corresponding dual combinations starting in adult CMT1A rats for 3 months. Motor endpoints were monitored over time, while the sensory endpoint was assessed at study end. In the dose-finding study, PXT3003-3 consistently increased the grip strength of the hindlimbs ((a); study end: two-way ANOVA on transformed data results as change from baseline: F_{Time} (1.1775, 168.7) = 243.5; $p < 0.0001$; F_{Group} (4, 95) = 5.315 $p = 0.0007$; $F_{\text{Time} \times \text{Group}}$ (8, 190) = 3.959 $p = 0.0002$ (b)), the bar holding time (c, d); and the hot plate reactivity at study end (one-way ANOVA $F(5, 114) = 35.32$ $p < 0.0001$ (e)). Dual combinations BCL/NTX-3, BCL/SRB-3, and NTX/SRB-3 were either not significantly effective or importantly, their activity was inferior to PXT3003-3 as recorded by the grip strength of the hindlimbs ((f); study end: two-way ANOVA results on transformed data as change from baseline: F_{Time} (1.775, 168.7) = 243.5; $p < 0.0001$; F_{Group} (4, 95) = 5.315 $p = 0.0007$; $F_{\text{Time} \times \text{Group}}$ (8, 190) = 3.959 $p = 0.0002$ (g)), the bar holding time ((h); study end: two-way ANOVA results on transformed data: F_{Time} (1.384, 131.5) = 39.08, $p < 0.0001$; F_{Group} (4, 95) = 4.068 $p = 0.0044$; $F_{\text{Time} \times \text{Group}}$ (8, 190) = 4.128, $p = 0.0001$ (i)), and the hot plate reactivity at study end (one-way ANOVA result: $F(5, 114) = 56.67$, $p < 0.0001$ (j)). $n = 19$ – 21 per group. a, c, d, f, and h; t test. b, g, and i; two-way ANOVA + Dunnett. e and j; one-way ANOVA + Dunnett. # $p < 0.05$ CMT1A placebo versus WT placebo; * $p < 0.05$ CMT1A any treatment versus CMT1A placebo; + $p < 0.05$ CMT1A PXT3003-3 versus CMT1A dual combinations; dot plots and means, otherwise means and SD (a, c, f, and h)

placebo (Figure 2e). For CMT1A rats treated with the three highest PXT3003 dosages we observed a significantly faster reaction time reaching a maximum for PXT3003-3 when compared to CMT1A placebo (10.0 ± 2.2 s for PXT3003-2, 8.6 ± 1.8 s for PXT3003-3, and 9.1 ± 1.8 s for PXT3003-4) (Figure 2e).

Thus, PXT3003-3 dosage was consistently the most effective on motor and sensory endpoints and therefore was selected to compare the superiority of PXT3003 to its two-drug combinations in a further study.

In this second study, grip strength measurements confirmed the weakness of the hindlimbs in CMT1A placebo rats throughout the entire 3 months study period when compared to WT placebo, and PXT3003-3 treated CMT1A rats again continuously increased in muscle strength until study end (Figure 2f). Here, CMT1A placebo rats showed a lower muscle strength of 7.1 ± 1.2 N compared to 12.4 ± 0.9 N in WT placebo (Figure S2c), and CMT1A rats treated with PXT3003-3 significantly increased in grip strength to 9.0 ± 1.4 N (Figure 2g and Figure S2c). Generally, none of the corresponding two-drug combinations significantly improved muscle weakness in CMT1A rats when compared to CMT1A placebo, and importantly remained significantly weaker compared to PXT3003-3 treated rats (Figure 2g). We measured 7.2 ± 1.1 N for BCL/NTX-3, 7.7 ± 1.8 N for BCL/SRB-3, and 7.4 ± 1.8 N for NTX/SRB-3 (Figure S2c).

Throughout the entire study period, the bar holding test confirmed the deficits in CMT1A placebo rats compared to WT placebo, and PXT3003-3 treated CMT1A rats continuously improved bar holding time until study end (Figure 2h). At this time point, CMT1A placebo rats showed a lower bar holding time of 22.0 ± 36.1 s compared to 180.0 ± 0.0 s in WT placebo. CMT1A rats treated with PXT3003-3 significantly improved bar holding performance to 49.2 ± 40.4 s (Figure 2h,i). Again, none of the corresponding dual combinations significantly improved bar holding performance in CMT1A rats when compared to CMT1A placebo, whereas PXT3003-3 was not only significantly efficacious versus placebo but also had a significantly superior effect to all three dual combinations at study end (Figure 2i). We measured 26.8 ± 32.7 s for BCL/NTX-3, 16.8 ± 13.9 s for BCL/SRB-3, and 15.6 ± 11.9 s for NTX/SRB-3 (Figure S2d).

The inclined plane behavior test demonstrated again high variability but confirmed higher deficit scores in CMT1A placebo rats throughout the study period reaching 0.5 ± 0.5 compared to 0.0 ± 0.0

in WT placebo at study end (Figure S2e). CMT1A rats treated with PXT3003-3 and BCL/NTX-3 improved the deficit score compared to CMT1A placebo rats (0.12 ± 0.34 and 0.13 ± 0.46 , respectively) (Figure S2f). However, and as expected, we did not observe any treatment effects when data were analyzed as change from baseline (Figure S2g).

Sensory measures at study end confirmed significantly delayed thermal reactivity in CMT1A placebo of 14.7 ± 2.4 s compared to 7.5 ± 0.6 s in WT placebo, and PXT3003-3 treated CMT1A rats confirmed their significant improvement of thermal reactivity to 9.1 ± 1.5 s (Figure 2j). Here, BCL/NTX-3 treated CMT1A rats also significantly improved thermal reactivity to 12.2 ± 2.0 s when compared to CMT1A placebo, but remained significantly inferior to PXT3003-3 therapeutic effect. The remaining two dual combinations did not significantly affect thermal reactivity in CMT1A rats and were significantly inferior when compared to PXT3003-3 therapy effect. We measured 14.4 ± 1.4 s for BCL/SRB-3 and 14.5 ± 2.5 s for NTX/SRB-3 (Figure 2j).

In summary, PXT3003-3 confirmed its effectiveness on motor and sensory endpoints and showed a significant superior efficacy compared to its dual combinations.

Body weights were monitored in both studies. At study ends, we observed in both studies body weight reductions in CMT1A placebo rats (464 ± 73 g and 475 ± 42 g, respectively) when compared to WT placebo (512 ± 37 g and 512 ± 38 g, respectively). Body weight was neither affected by PXT3003-1 (455 ± 54 g), PXT3003-2 (455 ± 43 g), PXT3003-3 (479 ± 59 g), PXT3003-4 (462 ± 57 g) nor by the corresponding dual combinations BCL/NTX-3 (472 ± 44 g), BCL/SRB-3 (469 ± 49 g), and NTX/SRB-3 (471 ± 46 g) (Figures S1h and S2h).

3.3 | PXT3003 marginally improves nerve pathology in CMT1A rats

Nerve effects were investigated for PXT3003-3 as it was consistently the most effective dosage and compared to the highest dose of PXT3003-4. Electrophysiological analyses of peripheral nerves were performed at study end. In tail nerve recordings generated in the dose-response study, CMT1A placebo rats showed a

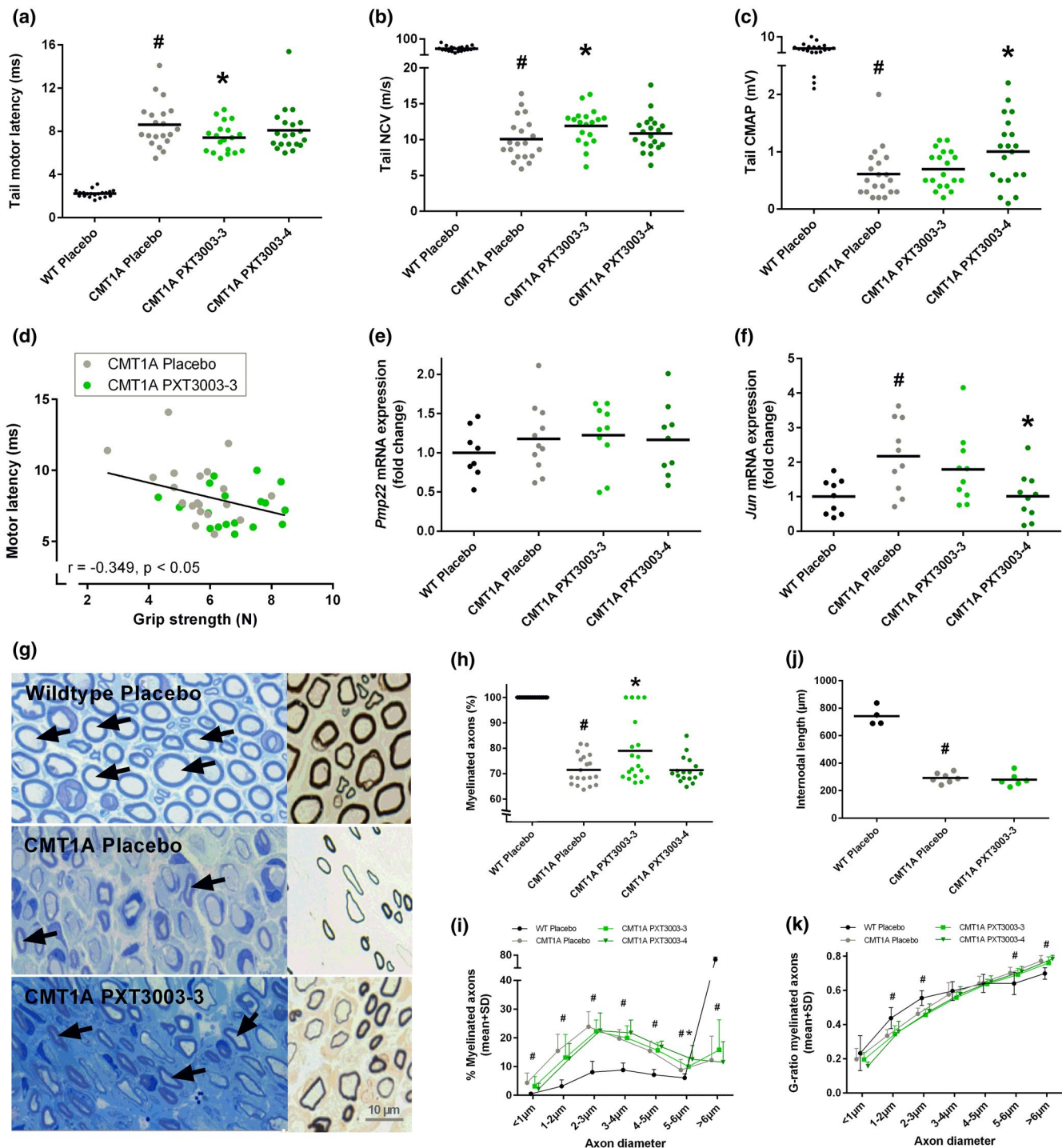


FIGURE 3 PXT3003 marginally improves nerve pathology in CMT1A rats. Motor latency was improved by PXT3003-3 in the tail after proximal stimulation (a), and motor latency and motor function correlated in placebo and PXT3003-3 treated CMT1A rats (d). Nerve conduction velocity (NCV) and proximal compound muscle action potentials (CMAP) were improved by PXT3003-3 (b) or PXT3003-4 (c), respectively. Transcriptional analysis showed missing therapy effects on *Pmp22* (non-significant) overexpression for any PXT3003 dose in CMT1A rats (e). PXT3003-4 reduced mRNA expression of the de-differentiation marker *Jun* (f). Light microscopic analysis in the femoral nerve stained with methylene blue/Azur II and by silver impregnation according to Gallyas (g) showed more total myelinated axons in CMT1A rats after PXT3003-3 therapy (h, and illustrated by black arrows in g) as well as an higher portion of large-caliber axons of 5–6 μm diameter after PXT3003-4 therapy (i). No therapy effects were observed on intermodal lengths (j) and myelin sheath thickness (k). $n = 4$ –20 per group; t tests; # $p < 0.05$ CMT1A placebo versus WT placebo; * $p < 0.05$ CMT1A PXT3003 versus CMT1A placebo; dot plots and means, otherwise means and SD (i and k)

significantly delayed motor latency of 8.6 ± 2.1 ms after proximal stimulation (Figure 3a), a decreased nerve conduction velocity (NCV) of 10.1 ± 2.9 m/s (Figure 3b) and reduced proximal compound muscle action potentials (CMAP) of 0.6 ± 0.4 mV when compared to WT placebo (2.2 ± 0.3 ms, 51.5 ± 12.9 m/s, and 4.5 ± 2.1 mV) (Figure 3c). PXT3003-3 significantly shortened motor latency delay to 7.4 ± 1.4 ms when compared to CMT1A placebo (Figure 3a) which significantly correlated with the motor function in these rats (Pearson $r = -0.349$, $p < 0.05$) (Figure 3d). Small significant effects were also observed on NCV (11.9 ± 2.5 m/s for PXT3003-3 treated CMT1A rats) and CMAP (1.0 ± 0.6 mV for PXT3003-4 treated CMT1A rats) when compared to CMT1A placebo (Figure 3b,c).

In the second experiment, significant electrophysiological effects were absent in tail recordings for PXT3003-3 and its dual combinations BCL/NTX-3, BCL/SRB-3, and NTX/SRB-3 (data not shown). However, in the sciatic nerve we observed a trend for improvement for motor latency for PXT3003-3 when distally stimulated in CMT1A rats ($p = 0.1$) (Figure S3a). Dual combinations BCL/NTX-3, BCL/SRB-3, and NTX/SRB-3 were not significantly effective on motor latency, NCV and CMAP in the sciatic nerve (Figure S3a–c).

Transcriptional analyses were performed in the sciatic nerve at 18 weeks. At this time point, CMT1A placebo rats revealed a low non-significant 1.2 ± 0.4 fold *Pmp22* overexpression in the dose-response study (Figure 3e), and we measured a low significant 1.3 ± 0.3 fold *Pmp22* overexpression in the second study (Figure S3d). Known de-differentiation markers *Jun* and *Sox2* were significantly upregulated in CMT1A placebo rats relative to wildtype level, we measured 2.2 ± 1.0 for *Jun* in the dose-response study (Figure 3f) and 2.1 ± 0.5 for *Sox2* in the second study (Figure S3e). Taking both studies into account, neither PXT3003-3 nor its three corresponding dual combinations BCL/NTX-3, BCL/SRB-3, and NTX/SRB-3 significantly affected mRNA expression of *Pmp22*, *Jun* and *Sox2* in treated CMT1A rats (Figure 3e,f and Figure S3d,e). We solely observed an isolated significant reduction of *Jun* mRNA expression by PXT3003-4 in CMT1A rats (1.0 ± 0.7) when compared to CMT1A placebo (Figure 3f).

Histological analyses were performed in the femoral nerve stained with methylene blue/Azur II and by silver impregnation according to Gallyas (Figure 3g). We observed less myelinated axons in CMT1A placebo rats ($71.5 \pm 5.8\%$) compared to WT placebo ($100.0 \pm 0.0\%$) in whole nerve cross sections (Figure 3h) and a relative loss of large-caliber axons when analyzing a subset of myelinated axons in more detail (Figure 3i). In the dose-finding study, PXT3003-3 significantly increased the percentage of total myelinated axons in CMT1A rats to $79.0 \pm 12.6\%$ (Figure 3h) but this effect could not be reproduced in the second study (Figure S3f). Dual combinations BCL/NTX-3, BCL/SRB-3, and NTX/SRB-3 did not affect total myelinated axons (Figure S3f). We further observed an isolated PXT3003-4 effect on the significantly increased percentage of 5–6 μ m large-caliber axons ($12.5 \pm 4.8\%$) when compared to CMT1A placebo ($8.8 \pm 3.7\%$) (Figure 3i). Under these conditions, we observed no PXT3003 effects on internodal myelin lengths (Figure 3j) or hyper/hypomyelination of small-caliber/large-caliber axons, respectively (Figure 3k).

3.4 | Improvement of neuromuscular junction pathology with PXT3003 therapy in CMT1A rats

Given the pronounced improvement of muscular functions in the absence of clear effects on myelination, we extended our analyses to the terminal neuromuscular unit. Histological analyses of neuromuscular pathology were performed in the gastrocnemius muscle. First, we stained for acetylcholine esterase to characterize the morphology of neuromuscular junctions (NMJ) in CMT1A rats (Figure 4a). Here, we observed significantly smaller NMJs (87.1 ± 12.0 μ m) (Figure 4c) and a significantly higher NMJ density (155 ± 83 per cm^2) in CMT1A placebo rats compared to WT placebo (97.7 ± 9.3 μ m and 89 ± 23 per cm^2 , respectively) (Figure 4d). PXT3003-3 treated CMT1A rats displayed amelioration of both, the NMJ size (101.3 ± 13.6 μ m) as well as the NMJ density (92 ± 21 per cm^2), by reaching the wildtype level (Figure 4c,d). Interestingly, we also observed a strong significant correlation between NMJ size and the sensory function in placebo and PXT3003-3 treated CMT1A rats (Pearson $r = -0.627$, $p < 0.001$) (Figure 4f).

We next performed immunohistological staining for neurofilaments and endplates in order to investigate terminal innervation of the NMJs (Figure 4b). CMT1A placebo rats were characterized by a significantly lower number of innervated NMJs ($78.7 \pm 12.8\%$) compared to WT placebo ($92.6 \pm 5.0\%$), and PXT3003-3 therapy in CMT1A was highly effective to significantly restore terminal innervation at the NMJs ($91.9 \pm 5.2\%$) toward the wildtype level (Figure 4e). Consistent with findings above, we observed a strong significant correlation between the NMJs innervation and the sensory function in these rats (Pearson $r = -0.539$, $p < 0.001$) (Figure 4g).

3.5 | PXT3003 improves muscle pathology in CMT1A rats

The percentage of angular atrophic muscle fibers was counted as a morphologic readout for neurogenic muscle atrophy (Figure 5a). In CMT1A rats, the percentage of angular fibers was significantly increased to $17.1 \pm 3.3\%$ when compared to WT placebo ($2.5 \pm 1.2\%$). PXT3003-3 therapy in CMT1A rats significantly reduced the percentage of angular muscle fibers to $9.4 \pm 5.4\%$ (Figure 5c).

For immunohistological analyses of muscle fiber subtyping (Figure 5b), we used myosin heavy chain (MHC) subtype specific antibodies differentiating between muscle fiber types IIa, IIb, and IIx. Here, we observed a loss of type IIb ($40.0 \pm 8.2\%$) versus an increase of type IIa muscle fibers ($20.0 \pm 12.2\%$) in CMT1A placebo rats when compared to WT placebo (50.3 ± 25.8 and $15.6 \pm 13.7\%$, respectively), although not significant. Furthermore, we observed a trend toward increased number of type IIa/IIx hybrid muscle fibers in CMT1A placebo rats ($10.3 \pm 11.9\%$) when compared to WT placebo ($3.3 \pm 6.5\%$) (Figure 5d). PXT3003-3 therapy in CMT1A rats significantly increased the percentage of type IIb muscle fibers to $59.3 \pm 13.0\%$ compared to CMT1A placebo rats. We also identified an increase in the percentage of type IIa ($10.0 \pm 5.2\%$) and type IIa/IIx hybrid muscle fibers after PXT3003-3 therapy ($0.5 \pm 1.3\%$) when

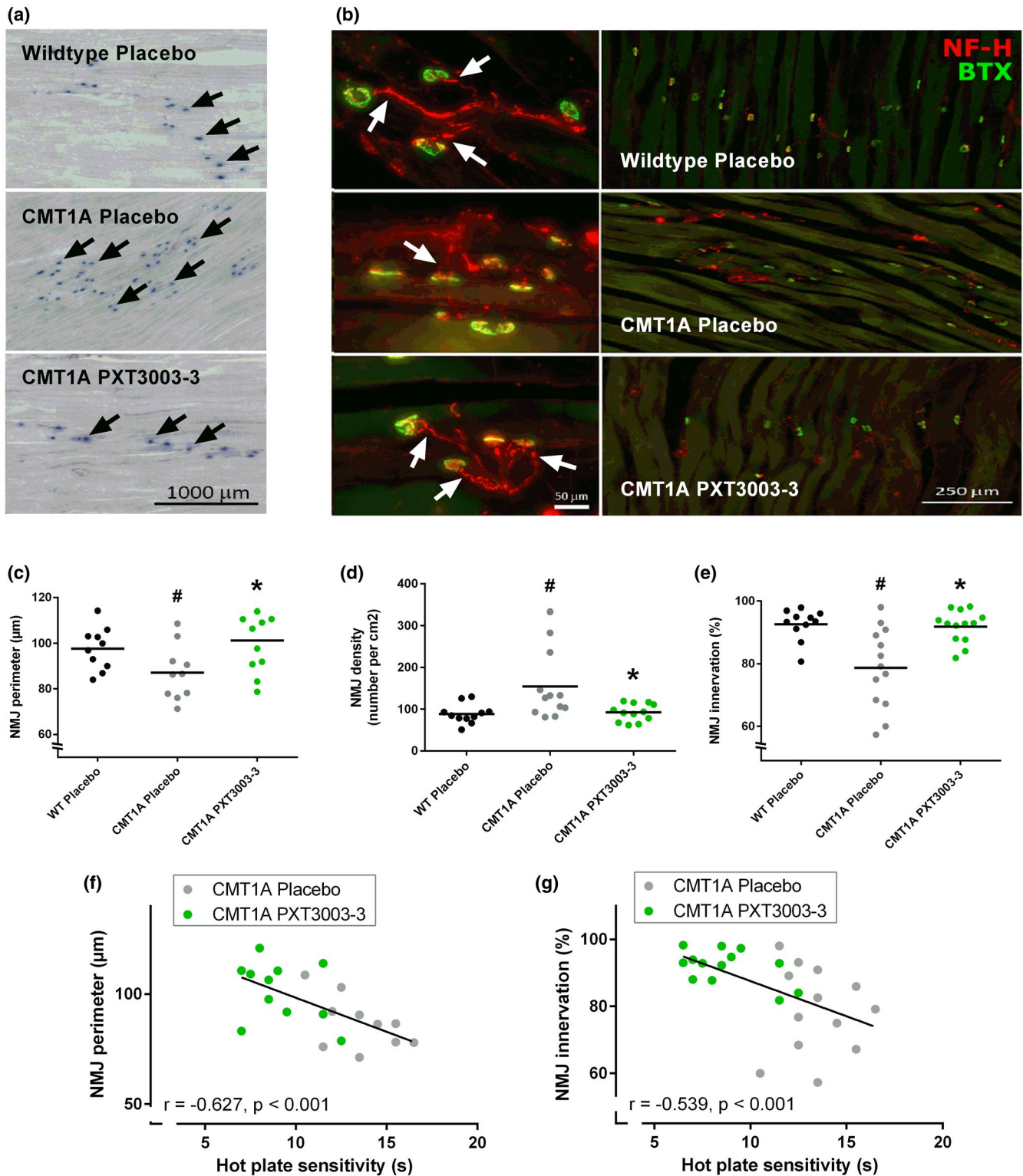


FIGURE 4 Restored NMJ pathology by PXT3003 therapy in CMT1A rats. Morphologic analyses of neuromuscular junctions (NMJ) were performed in the gastrocnemius muscle by cholinesterase staining (a, black arrows). PXT3003-3 therapy corrected the size (c) and amount of NMJs (d) in CMT1A rats. NMJ size and sensory function correlated in placebo and PXT3003-3 treated CMT1A rats (f). NMJ innervation was analyzed by double staining for neurofilament H (NF-H) and Alexa Fluor-conjugated α -bungarotoxin (BTX) in the gastrocnemius muscle (b, white arrows). PXT3003-3 therapy restored NMJ innervation in CMT1A rats (e), and NMJ innervation correlated with sensory function in placebo and PXT3003-3 treated rats (g). $n = 10$ –13 per group; t tests; # $p < 0.05$ CMT1A placebo versus WT placebo; * $p < 0.05$ CMT1A PXT3003 versus CMT1A placebo; dot plots and means

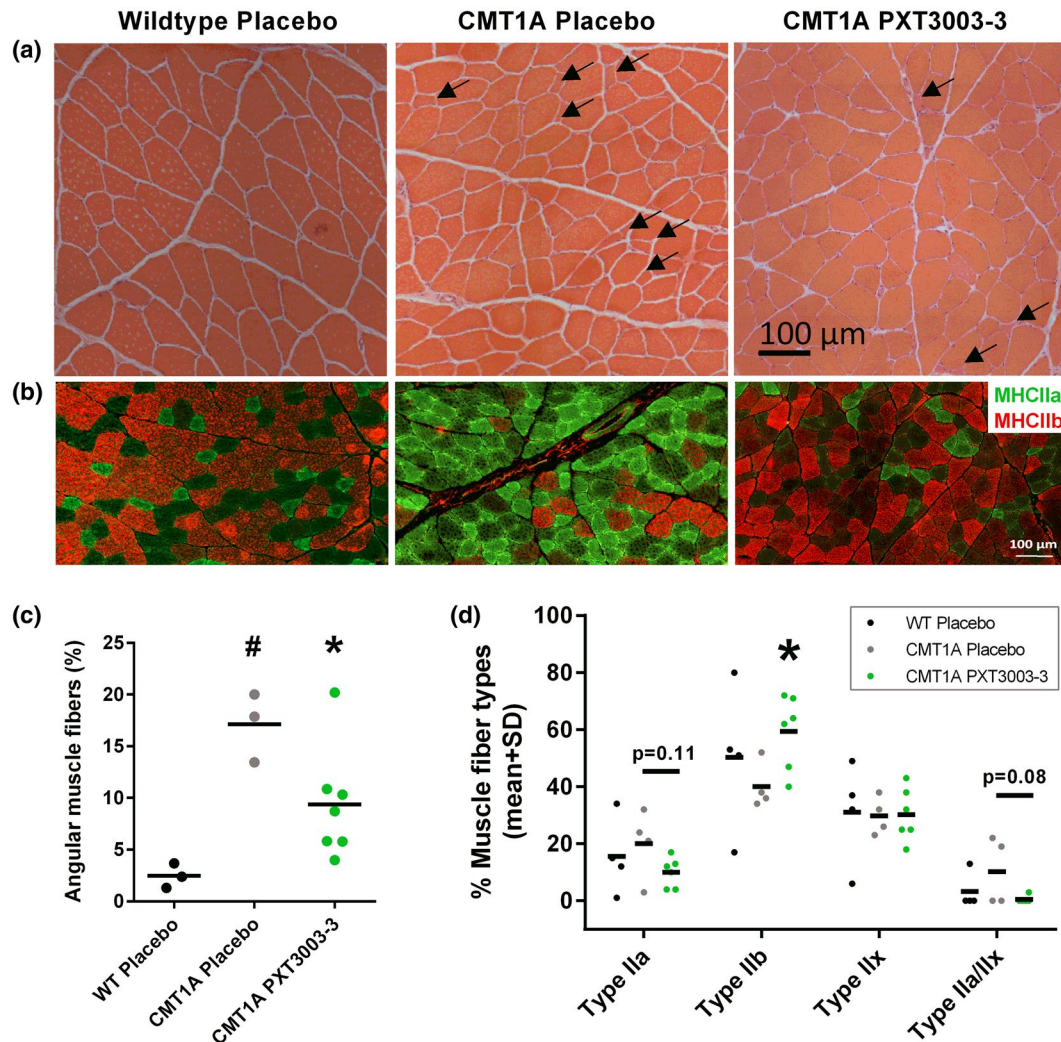


FIGURE 5 PXT3003 improved muscle pathology in CMT1A rats. Representative photographs of HE-stained sections of the gastrocnemius muscle (a) showing atrophic angular fibers (black arrows) in CMT1A rats (middle and right panels). The percentage of atrophic fibers was reduced upon PXT3003-3 therapy (c). Selected photographs of muscle fiber type IIa (MHCIIa, green) and IIb (MHCIIb, red) specific antibody staining in sections of the gastrocnemius muscle (b) highlighting less type IIb fibers in placebo-treated CMT1A rats (middle panel). PXT3003-3 improved disturbed type IIb fiber composition in CMT1A rats and tended also to improve type IIa and type IIa/IIx hybrid muscle fibers (d). $n = 3-7$ per group; t tests; # $p < 0.05$ CMT1A placebo versus WT placebo; * $p < 0.05$ CMT1A PXT3003 versus CMT1A placebo; dot plots and means (c and d)

compared to CMT1A placebo, although significance was not reached ($p = 0.11$ and $p = 0.08$, respectively) (Figure 5d).

Transcriptional analyses independently supported these immunohistological findings. We quantified muscle fiber type IIb specific mRNA expression in a subset of rats and measured for WT placebo a 1.1 ± 0.62 , for CMT1A placebo a 0.45 ± 0.41 and for CMT1A rats treated with PXT3003-3 a 1.0 ± 0.65 fold expression, in line with significantly more type IIb muscle fibers in CMT1A rats treated for 3 months with PXT3003-3 (Figure S3g).

4 | DISCUSSION

PXT3003 is a fixed-ratio drug combination of low-dose baclofen (BCL), naltrexone (NTX), and sorbitol (SRB). Previous preclinical studies in

CMT1A rats demonstrated that PXT3003 slows down or even partially prevent disease progression (Chumakov et al., 2014; Prukop et al., 2019). In CMT1A patients, PXT3003 was effective on clinical endpoints in a phase 2 study (Attarian et al., 2014, 2016), and effects were also confirmed in a first analysis of a phase 3 international study (Clinical Trials Register/Results, 2019). However, the contribution of the single components to the overall efficacy of PXT3003 remained elusive, and recent preclinical data suggested beneficial effects beyond improving the known nerve pathology (Prukop et al., 2019). To address these questions, we compared PXT3003 and its components in CMT1A rats and extended our analyses to the neuromuscular unit apart from the motoneuron, that is, the peripheral nerve, the neuromuscular junction (NMJ), and the muscle.

We used only male CMT1A rats to minimize the heterogeneity on motor endpoints due to gender-specific differences in body

weight and to keep animal numbers as low as needed to minimize animal's burden for ethical reasons. Despite this limitation, using only one sex is considered sufficient since gender differences were not observed in CMT1A rats on disease severity with regard to molecular, electrophysiological, histological, and phenotypical characteristics (Chumakov et al., 2014; Fledrich et al., 2012, 2014, 2018; Meyer zu Horste et al., 2007; Prukop et al., 2019; Sereda et al., 1996; Sereda, Meyer zu Hörste, Suter, Uzma, & Nave, 2003; Sociali et al., 2016). Moreover, no gender effect was reported in male and female CMT1A rats treated independently with Onapristone (Meyer zu Horste et al., 2007; Sereda et al., 2003), and no gender effect was observed in CMT1A patients after therapy with PXT3003 (Attarian et al., 2014, 2016) (Clinical Trials Register/Results, 2019).

4.1 | How does the PXT3003 effect relate to its single components?

In order to investigate the synergistic effect of PXT3003, we established DRG sensory neuron/Schwann cell co-cultures derived from *Pmp22* transgenic rats. We tested the dose-response on myelination of the single components to identify the sub-active doses for each drug. These low doses were then combined to generate PXT3003 mixes and to identify the most potent combination on myelination. Treatment over 4 weeks with sub-active concentrations promoted myelination when given as PXT3003 as shown for both, PMP22 and MBP as markers of myelination. In contrast, single drugs and dual combinations of BCL, NTX, and SRB were not significantly effective at the corresponding doses. Furthermore, the PXT3003 effect even exceeded the maximum effects of its single drugs and herewith demonstrated its superiority compared to the single components. Thus, BCL, NTX, and SRB acted synergistically to improve myelination which highlights the advantage of combining drugs at low doses.

Second, we applied a clinically relevant, that is, translational study design with a chronic dosing in affected CMT1A rats to mimic adult CMT1A patients suffering from the disease. To identify the most effective dosage multiple PXT3003 dosages were tested by monitoring motor and sensory endpoints. PXT3003 reproducibly improved the grip strength, bar holding performance, and thermal sensitivity of CMT1A rats whereas its corresponding two-component combinations BCL/NTX, BCL/SRB, and NTX/SRB did not when compared to PXT3003. We could not consistently confirm the effects of PXT3003 in the inclined plane test. In line with a recent report in younger CMT1A rats (Prukop et al., 2019), our data here confirmed that this test shows high variability over time when animals gain weight. Therefore, this test should be avoided to assess motor function in adult CMT1A rats in future studies.

We did not test single components in CMT1A rats since we did not expect exceeding effects over the dual combinations based on our *in vitro* results, and thus for ethical reasons. Since dual combinations were inferior to PXT3003 in behavioral analyses, further analyses of NMJs and muscles were not performed for BCL/NTX, BCL/SRB, and NTX/SRB.

Our data demonstrate that there is a synergistic *in vitro* effect of PXT3003 on myelination, which is mirrored *in vivo* by its superior efficacy on behavioral performance compared to any of the two-drug combinations. These results prove the combined positive effect of BCL, NTX, and SRB in PXT3003 and emphasize the therapeutic value of combining repurposed drugs at low doses to alleviate symptoms while allowing to dramatically lower the occurrence of side effects during chronic treatment (Chumakov et al., 2014, 2015; Hajj et al., 2015; Halatsch et al., 2019; Prukop et al., 2019).

4.2 | What is the mechanism responsible for the increased muscle strength in CMT1A rats after PXT3003 treatment?

Previous preclinical studies in CMT1A rats demonstrated PXT3003 effects on *Pmp22* mRNA expression, myelination and axonal loss leading to an improved motor and sensory functions (Chumakov et al., 2014). When PXT3003 was administered early postnatally for a short-term during the critical time window of myelination, long-lasting and continuous increasing effects on muscle strength were observed, even after cessation of treatment, almost reaching wildtype levels (Prukop et al., 2019). In the present study regimen, PXT3003 treatment resulted in a profound improvement of motor and sensory functions, in the absence of major effects on myelin thickness and intermodal length. While we cannot rule out that longer treatment schedules may demonstrate more conclusive effects on myelination, the prominent and reproducible improvement of muscle and sensory function in CMT1A rats was not fully reflected by ameliorations of electrophysiological, axonal, or myelin parameters, reminiscent of previous studies in CMT1A rats treated with progesterone antagonists (Meyer zu Horste et al., 2007). Thus, effects on electrophysiology and histology were weak or even failed reproduction, most probably due of the weak effect observed that may be caused by the late initiation and short duration of the treatment. Importantly, muscle and sensory function increased beyond stabilization in adult affected CMT1A rats after long-term PXT3003 treatment, although not reaching wildtype levels contrary to early treatment start in young unaffected CMT1A rats (Prukop et al., 2019). This is in line with published PXT3003 therapy in adult affected CMT1A patients, which demonstrated improvement of clinical readout beyond stabilization as well (Attarian et al., 2014, 2016). If translated to CMT1A patients, PXT3003 therapy can be successfully initiated in affected adulthood but should preferentially begin as early as possible (e.g., in childhood) to most efficiently slow down, improve or even prevent the progression of the disease.

Moreover, weak correlations between electrophysiological parameters and clinical endpoints, for instance in the Charcot-Marie-Tooth Examination Score (CMTES), were also noticed in CMT1A patients (Manganelli et al., 2016). Of note, clinical assessments of efficacious therapies such as immunoglobulins in chronic inflammatory demyelinating polyradiculoneuropathy failed to achieve significant positive effects on electrophysiological endpoints although motor

performance was improved (Bril et al., 2009; Hughes et al., 2008). The CMAP amplitude is a measure of the number and size of active muscle fibers, and CMAP reduction suggests a loss of motor axons and neurons. However, conduction blocks preceding axonal loss result in CMAP reductions as well (Uncini & Kuwabara, 2015; Van Dijk, van Bente, Kramer, & Stegeman, 1999), and CMAP often not directly correlated with the extent of axonal loss which questions its use as an indicator of therapeutic effects (Lewis, Li, Fuerst, Shy, & Krajewski, 2003). In contrast to nerve conduction velocity (NCV), motor latency is a direct readout of muscle innervation by nerve terminals (Dyck & Thomas, 2005; Preston & Shapiro, 2013). Motor latency is defined as the time from the stimulus delivery to the initial signal of the CMAP and contains three temporal components, which represent three structural components of the motor unit. These are the time of nerve conduction from the site of the stimulus to the NMJ, the delay in transmission at the NMJ, and then the depolarization across the muscle fiber (Van Dijk et al., 1999).

Motor latency was ameliorated after PXT3003 treatment and strongly correlated with motor function improvement, similar to other experimental therapeutic trials in CMT1A rats (Sociali et al., 2016) and to the exploratory clinical phase 2 study in CMT1A patients (Attarian et al., 2014, 2016). The observed effect on motor latency, in the absence of myelin restoration with regard to myelin thickness and intermodal length, let us hypothesize that PXT3003 effects on muscle strength may be conveyed via an increase in functional NMJs. Indeed, the PXT3003 treatment increased the number of innervated, that is, functional, NMJs in CMT1A rats. The reduced NMJs size in CMT1A rats may be interpreted as a degenerating atrophic process due to diminished terminal innervation (Ang et al., 2010), and the observed restoration of the NMJs size by PXT3003 may be explained by the improved innervation. Also, the sensory behavior correlated with the number of innervated NMJs and NMJ size. Although the correlations between NMJ innervation and the sensory function are not obvious, they may reflect a general improved terminal innervation of afferent nerves to their endorgans, that is, the cutaneous receptors (which have not been examined in this study) in analogy to NMJs in the muscle. Further investigations of PXT3003 effects on afferent nerves are warranted to understand the improved sensory function in CMT1A rats. Axonal sprouting with partial axonal overgrowth can be seen as an attempt to improve the function of the damaged components of the motor unit through structural restoration (Schäfer & Wernig, 1998). However, despite mechanisms such as reinnervation, remyelination, and axonal sprouting, studies have shown that these intrinsic processes are insufficient to fully restore muscular function (Ang et al., 2010). We note that CMT1A rats display an increased area of axonal mitochondria in electron micrographs of femoral nerve cross sections which was corrected toward wildtype levels in animals treated with PXT3003 (data not shown). We thus hypothesize that PXT3003 improves the metabolic support of axons which then may improve terminal innervation at the NMJ by unknown mechanisms, for example, stabilization of existing terminal branches, protection from destabilization, pathological remodeling, promotion of reinnervation, primary axonal, or

support of terminal Schwann cells. However, any effects regarding myelination that may contribute to the *in vivo* phenotype cannot be generally ruled out for the given *in vivo* treatment regimen. Marginal effects were partially observed for NCV improvement and the number of myelinated axons as well, which may become more evident if we had treated longer. We note that the improved myelination by PXT3003 *in vitro* fits well to increased myelination described early treatment regime in young rats (Prukop et al., 2019).

Finally, we observed a higher density of total NMJs (irrespective of innervation) in CMT1A rats being restored by PXT3003 treatment, which at a first view may counter the analysis of innervated NMJs. Nevertheless, the amount of total NMJs may be interpreted as an indirect measure of muscle atrophy and was previously shown to vary in time and muscle groups in *Pmp22* transgenic mice (Ang et al., 2010; Fledrich et al., 2014). These data fit well to our findings in the muscle although its interpretation remains limited due to small given sample sizes. Angular muscle fibers are considered as an indirect parameter of neurogenic atrophy (Ericson, Ansved, & Borg, 1998) which are increased in CMT1A rats, consistent with CMT1A patients. PXT3003 treatment reduced the number of angular structures and caused a shift toward fast contracting type IIb muscle fibers. The NMJ is a known critical region of nerve-muscle communication and NMJ destabilization may cause a switch from fast to slow contracting muscle fibers in neuromuscular disease (Lepore, Casola, Dobrowolny, & Musarò, 2019). Cross-innervation experiments demonstrated that muscle fiber types are sensitive to the activity patterns presented via the innervating axons and may alter their contractile properties to match the firing patterns (Lee, 2019). Thus, the function of NMJ seems to play a decisive role in the development of motor strength in CMT1A which appears uncoupled from the degree of peripheral nerve myelination and which may constitute a new pharmacological target for PXT3003 therapy in adult animals (Prukop et al., 2019). Beyond its potential effect on NMJs, the authors cannot rule out a direct activity of PXT3003 on muscle cells by activation of IGF-1R signaling via opioid receptors (Evans, Tunncliffe, Knights, Bailey, & Smith, 2001; Olanas, Dedoni, & Onali, 2011; Scicchitano, Rizzuto, & Musarò, 2009), that may improve the muscle function in CMT1A. Further investigations are warranted.

There were no effects detected on *Pmp22* mRNA expression by PXT3003 in our study design, which was contrary to previous observations (Chumakov et al., 2014; Prukop et al., 2019). However, we showed before that the level of *Pmp22* overexpression decreases during adulthood (Fledrich et al., 2014), and accordingly, was low in 18 weeks old CMT1A rats in this study. Thus, we cannot rule out that therapy effects were indeed not present or just being masked by developmental reasons at study end. A longer treatment duration with PXT3003 may be needed to achieve a better understanding on physiological, electrophysiological, and molecular deficits observed in CMT1A rats. If NMJ denervation was a common axonal feature of CMT disease leading to muscle atrophy, weakness, and independent of Schwann cell *PMP22* duplication, putative therapeutic effects could be assumed even beyond CMT1A. However, to test this hypothesis, further preclinical and clinical proof-of-concept studies are required.

We conclude that baclofen, naltrexone, and sorbitol synergistically contribute to the therapeutic effect of PXT3003 in CMT1A disease. PXT3003 supports axonal function independent from restoration of myelination deficits, but improves the functional recovery of NMJ and hence muscle innervation, which ultimately increases muscle strength in adult CMT1A rats.

DECLARATION OF TRANSPARENCY

The authors, reviewers and editors affirm that in accordance to the policies set by the *Journal of Neuroscience Research*, this manuscript presents an accurate and transparent account of the study being reported and that all critical details describing the methods and results are present.

ACKNOWLEDGMENTS

We thank C. Maack, I. Iben, and B. Veith for excellent technical assistance in histological and biomolecular processing, and M. Wehe and D. Funk for excellent animal care. We thank Dr. Ilya Chumakov who participated in the selection of sorbitol contained in PXT3003.

CONFLICT OF INTEREST

This project was financially supported by Pharnext who additionally provided support in the form of salaries for its employees LB, AB, JL, GP, PR, SN, RH, and DCo. MWS, TP, and KAN acted as consultants to Pharnext.

AUTHOR CONTRIBUTIONS

All mentioned authors contributed to this work. *Conceptualization*, T.P., R.H., and M.W.S.; *Methodology*, T.P., R.H., and M.W.S.; *Candidate Drugs*, S.N.; *Validation*, T.P., S.W., A.B.-F., J.Z., A.B., and L.B.; *Formal Analysis*, T.P., S.W., L.B., A.B., D.E., J.Z., J.L., P.R., and R.H.; *Investigation*, S.W., D.E., K.J., J.A., L.W., S.Q., L.L., and G.P.; *Writing – Original Draft*, T.P., M.B., R.H., and M.W.S.; *Writing – Review & Editing*, T.P., S.W., L.B., D.E., D.Cz., J.Z., J.S., A.B., M.H.S., K.-A.N., R.H., D.Co., and M.W.S.; *Visualization*, T.P., S.W. and L.B.; *Supervision*, T.P., R.H., and M.W.S.

PEER REVIEW

The peer review history for this article is available at <https://publons.com/publon/10.1002/jnr.24679>.

DATA AVAILABILITY STATEMENT

The data that support the findings of this study are available from the corresponding author upon reasonable request.

ORCID

Thomas Prukop  <https://orcid.org/0000-0001-8210-9277>

REFERENCES

Ang, E.-T., Schäfer, R., Baltensperger, R., Wernig, A., Celio, M., & Oliver, S. S. (2010). Motor axonal sprouting and neuromuscular junction

- loss in an animal model of Charcot-Marie-Tooth disease. *Journal of Neuropathology and Experimental Neurology*, 69(3), 281–293. <https://doi.org/10.1097/NEN.0b013e3181d1e60f>
- Attarian, S., Vallat, J.-M., Magy, L., Funalot, B., Gonnaud, P.-M., Lacour, A., ... Cohen, D. (2014). An exploratory randomised double-blind and placebo-controlled phase 2 study of a combination of baclofen, naltrexone and sorbitol (PXT3003) in patients with Charcot-Marie-Tooth disease type 1A. *Orphanet Journal of Rare Diseases*, 9, 199. <https://doi.org/10.1186/s13023-014-0199-0>
- Attarian, S., Vallat, J.-M., Magy, L., Funalot, B., Gonnaud, P.-M., Lacour, A., ... Cohen, D. (2016). Erratum to: An exploratory randomised double-blind and placebo-controlled phase 2 study of a combination of baclofen, naltrexone and sorbitol (PXT3003) in patients with Charcot-Marie-Tooth disease type 1A. *Orphanet Journal of Rare Diseases*, 11(1), 92. <https://doi.org/10.1186/s13023-016-0463-6>
- Brennan, K. M., Bai, Y., & Shy, M. E. (2015). Demyelinating CMT—what's known, what's new and what's in store? *Neuroscience Letters*, 596, 14–26. <https://doi.org/10.1016/j.neulet.2015.01.059>
- Bril, V., Katzberg, H., Donofrio, P., Banach, M., Dalakas, M. C., Deng, C., ... Van Doorn, P. A. (2009). Electrophysiology in chronic inflammatory demyelinating polyneuropathy with IIGIV. *Muscle & Nerve*, 39(4), 448–455. <https://doi.org/10.1002/mus.21236>
- Callizot, N., Combes, M., Steinschneider, R., & Poindron, P. (2011). A new long term in vitro model of myelination. *Experimental Cell Research*, 317(16), 2374–2383. <https://doi.org/10.1016/j.yexcr.2011.07.002>
- Choudhary, S., Save, S. N., Kishore, N., & Hosur, R. V. (2016). Synergistic inhibition of protein fibrillation by proline and sorbitol: Biophysical investigations. *PLoS One*, 11(11), e0166487. <https://doi.org/10.1371/journal.pone.0166487>
- Chumakov, I., Milet, A., Cholet, N., Primas, G., Boucard, A., Pereira, Y., ... Cohen, D. (2014). Polytherapy with a combination of three repurposed drugs (PXT3003) down-regulates Pmp22 over-expression and improves myelination, axonal and functional parameters in models of CMT1A neuropathy. *Orphanet Journal of Rare Diseases*, 9, 201. <https://doi.org/10.1186/s13023-014-0201-x>
- Chumakov, I., Nabitochkin, S., Cholet, N., Milet, A., Boucard, A., Toulorge, D., ... Cohen, D. (2015). Combining two repurposed drugs as a promising approach for Alzheimer's disease therapy. *Scientific Reports*, 5, 7608. <https://doi.org/10.1038/srep07608>
- Clinical Trials Register/Results. (2019). Clinical trial results: International, multi-center, randomized, double-blind, placebo-controlled phase III study assessing in parallel groups the efficacy and safety of 2 doses of PXT3003 in patients with Charcot-Marie-Tooth disease type 1A treated for 15 months. Retrieved from <https://www.clinicaltrialsregister.eu/ctr-search/trial/2015-002378-19/results>
- Crain, S. M., & Shen, K. F. (2001). Acute thermal hyperalgesia elicited by low-dose morphine in normal mice is blocked by ultra-low-dose naltrexone. *Unmasking Potent Opioid Analgesia. Brain Research*, 888(1), 75–82. [https://doi.org/10.1016/S0006-8993\(00\)03010-9](https://doi.org/10.1016/S0006-8993(00)03010-9)
- Dyck, P. J., & Thomas, P. K. (Eds.). (2005). *Peripheral neuropathy* (4th ed.). Philadelphia, PA: Saunders. Retrieved from <http://www.sciencedirect.com/science/book/9780721694917>
- Ericson, U., Ansved, T., & Borg, K. (1998). Charcot-Marie-Tooth disease—Muscle biopsy findings in relation to neurophysiology. *Neuromuscular Disorders*, 8(3–4), 175–181. [https://doi.org/10.1016/S0960-8966\(98\)00018-2](https://doi.org/10.1016/S0960-8966(98)00018-2)
- Evans, A. A. L., Tunnicliffe, G., Knights, P., Bailey, C. J., & Smith, M. E. (2001). Delta opioid receptors mediate glucose uptake in skeletal muscles of lean and obese-diabetic (Ob/Ob) mice. *Metabolism*, 50(12), 1402–1408. <https://doi.org/10.1053/meta.2001.28158>
- Fledrich, R., Abdelaal, T., Rasch, L., Bansal, V., Schütza, V., Brügger, B., ... Sereda, M. W. (2018). Targeting myelin lipid metabolism as a potential therapeutic strategy in a model of CMT1A neuropathy. *Nature Communications*, 9(1), 3025. <https://doi.org/10.1038/s41467-018-05420-0>

- Fledrich, R., Akkermann, D., Schütza, V., Abdelaal, T. A., Hermes, D., Schäffner, E., ... Stassart, R. M. (2019a). NRG1 type I dependent autocrine stimulation of schwann cells in onion bulbs of peripheral neuropathies. *Nature Communications*, 10(1), 1467. <https://doi.org/10.1038/s41467-019-09385-6>
- Fledrich, R., Akkermann, D., Schütza, V., Abdelaal, T. A., Hermes, D., Schäffner, E., ... Stassart, R. M. (2019b). Publisher correction: NRG1 type I dependent autocrine stimulation of schwann cells in onion bulbs of peripheral neuropathies. *Nature Communications*, 10(1), 1840. <https://doi.org/10.1038/s41467-019-09886-4>
- Fledrich, R., Schlotter-Weigel, B., Schnizer, T. J., Wichert, S. P., Stassart, R. M., Meyer zu Hörste, G., ... Sereda, M. W. (2012). A rat model of Charcot-Marie-Tooth disease 1A recapitulates disease variability and supplies biomarkers of axonal loss in patients. *Brain*, 135(Pt 1), 72–87. <https://doi.org/10.1093/brain/awr322>
- Fledrich, R., Stassart, R. M., Klink, A., Rasch, L. M., Prukop, T., Haag, L., ... Sereda, M. W. (2014). Soluble neuregulin-1 modulates disease pathogenesis in rodent models of Charcot-Marie-Tooth disease 1A. *Nature Medicine*, 20(9), 1055–1061. <https://doi.org/10.1038/nm.3664>
- Foucquier, J., & Guedj, M. (2015). Analysis of drug combinations: Current methodological landscape. *Pharmacology Research & Perspectives*, 3(3), e00149. <https://doi.org/10.1002/prp2.149>
- Hajj, R., Milet, A., Toulorge, D., Cholet, N., Laffaire, J., Foucquier, J., ... Cohen, D. (2015). Combination of acamprosate and baclofen as a promising therapeutic approach for Parkinson's disease. *Scientific Reports*, 5, 16084. <https://doi.org/10.1038/srep16084>
- Halatsch, M.-E., Kast, R. E., Dwucet, A., Hlavac, M., Heiland, T., Westhoff, M.-A., ... Karpel-Massler, G. (2019). Bcl-2/Bcl-XL inhibition predominantly synergistically enhances the anti-neoplastic activity of a low-dose CUSP9 repurposed drug regime against glioblastoma. *British Journal of Pharmacology*, 176(18), 3681–3694. <https://doi.org/10.1111/bph.14773>
- Hughes, R. A. C., Donofrio, P., Bril, V., Dalakas, M. C., Deng, C., Hanna, K., ... van Doorn, P. A. (2008). Intravenous immune globulin (10% caprylate-chromatography purified) for the treatment of chronic inflammatory demyelinating polyradiculoneuropathy (ICE study): A randomised placebo-controlled trial. *Lancet Neurology*, 7(2), 136–144. [https://doi.org/10.1016/S1474-4422\(07\)70329-0](https://doi.org/10.1016/S1474-4422(07)70329-0)
- Hyttek, S. D., McLaughlin, P. J., Lang, C. M., & Zagon, I. S. (1996). Inhibition of human colon cancer by intermittent opioid receptor blockade with naltrexone. *Cancer Letters*, 101(2), 159–164. [https://doi.org/10.1016/0304-3835\(96\)04119-5](https://doi.org/10.1016/0304-3835(96)04119-5)
- Lee, Y. I. (2019). Differences in the constituent fiber types contribute to the intermuscular variation in the timing of the developmental synapse elimination. *Scientific Reports*, 9(1), 8694. <https://doi.org/10.1038/s41598-019-45090-6>
- Lepore, E., Casola, I., Dobrowolny, G., & Musarò, A. (2019). Neuromuscular junction as an entity of nerve-muscle communication. *Cells*, 8(8), 906. <https://doi.org/10.3390/cells8080906>
- Lewis, R. A., Li, J., Fuerst, D. R., Shy, M. E., & Krajewski, K. (2003). Motor unit number estimate of distal and proximal muscles in Charcot-Marie-Tooth disease. *Muscle & Nerve*, 28(2), 161–167. <https://doi.org/10.1002/mus.10419>
- Lewis, R. A., Mcdermott, M. P., Herrmann, D. N., Hoke, A., Clawson, L. L., Siskind, C., ... Shy, M. E. (2013). High-dosage ascorbic acid treatment in Charcot-Marie-Tooth disease type 1A: Results of a randomized, double-masked, controlled trial. *JAMA Neurology*, 70(8), 981–987. <https://doi.org/10.1001/jamaneurol.2013.3178>
- Li, J., Parker, B., Martyn, C., Natarajan, C., & Guo, J. (2013). The PMP22 gene and its related diseases. *Molecular Neurobiology*, 47(2), 673–698. <https://doi.org/10.1007/s12035-012-8370-x>
- Lupski, J. R., de Oca-Luna, R. M., Slaugenhaupt, S., Pentao, L., Guzzetta, V., Trask, B. J., ... Patel, P. I. (1991). DNA duplication associated with Charcot-Marie-Tooth disease type 1A. *Cell*, 66(2), 219–232. [https://doi.org/10.1016/0092-8674\(91\)90613-4](https://doi.org/10.1016/0092-8674(91)90613-4)
- Lupski, J. R., & Garcia, C. A. (1992). Molecular genetics and neuropathology of Charcot-Marie-Tooth disease type 1A. *Brain Pathology*, 2(4), 337–349. <https://doi.org/10.1111/j.1750-3639.1992.tb00710.x>
- Magnaghi, V., Ballabio, M., Cavarretta, I. T. R., Froestl, W., Lambert, J. J., Zucchi, I., & Melcangi, R. C. (2004). GABAB receptors in Schwann cells influence proliferation and myelin protein expression. *European Journal of Neuroscience*, 19(10), 2641–2649. <https://doi.org/10.1111/j.0953-816X.2004.03368.x>
- Magnaghi, V., Ballabio, M., Consoli, A., Lambert, J. J., Roglio, I., & Melcangi, R. C. (2006). GABA receptor-mediated effects in the peripheral nervous system: A cross-interaction with neuroactive steroids. *Journal of Molecular Neuroscience*, 28(1), 89–102. <https://doi.org/10.1385/JMN:28:1:89>
- Manganelli, F., Pisciotto, C., Reilly, M. M., Tozza, S., Schenone, A., Fabrizi, G. M., ... Santoro, L. (2016). Nerve conduction velocity in CMT1A: What else can we tell? *European Journal of Neurology*, 23(10), 1566–1571. <https://doi.org/10.1111/ene.13079>
- Meyer zu Horste, G., Prukop, T., Liebetanz, D., Mobius, W., Nave, K.-A., & Sereda, M. W. (2007). Antiprogesterone therapy uncouples axonal loss from demyelination in a transgenic rat model of CMT1A neuropathy. *Annals of Neurology*, 61(1), 61–72. <https://doi.org/10.1002/ana.21026>
- Mittendorf, K. F., Marinko, J. T., Hampton, C. M., Ke, Z., Hadziselimovic, A., Schleich, J. P., ... Ohi, M. D. (2017). Peripheral myelin protein 22 alters membrane architecture. *Science Advances*, 3(7), e1700220. <https://doi.org/10.1126/sciadv.1700220>
- Murphy, S. M., Laura, M., Fawcett, K., Pandraud, A., Liu, Y.-T., Davidson, G. L., ... Reilly, M. M. (2012). Charcot-Marie-Tooth disease: Frequency of genetic subtypes and guidelines for genetic testing. *Journal of Neurology, Neurosurgery, and Psychiatry*, 83(7), 706–710. <https://doi.org/10.1136/jnnp-2012-302451>
- Nicks, J. R., Lee, S., Kostamo, K. A., Harris, A. B., Sookdeo, A. M., & Notterpek, L. (2013). Long-term analyses of innervation and neuromuscular integrity in the Trembler-J mouse model of Charcot-Marie-Tooth disease. *Journal of Neuropathology and Experimental Neurology*, 72(10), 942–954. <https://doi.org/10.1097/NEN.0b013e3182a5f96e>
- Olianas, M. C., Dedoni, S., & Onali, P. (2011). δ -Opioid receptors stimulate GLUT1-mediated glucose uptake through Src- and IGF-1 receptor-dependent activation of PI3-kinase signalling in CHO cells. *British Journal of Pharmacology*, 163(3), 624–637. <https://doi.org/10.1111/j.1476-5381.2011.01234.x>
- Paquette, J., Olmstead, M. C., & Olmstead, M. (2005). Ultra-low dose naltrexone enhances cannabinoid-induced antinociception. *Behavioural Pharmacology*, 16(8), 597–603. <https://doi.org/10.1097/00008877-200512000-00001>
- Pareyson, D., Reilly, M. M., Schenone, A., Fabrizi, G. M., Cavallaro, T., Santoro, L., ... Solari, A. (2011). Ascorbic acid in Charcot-Marie-Tooth disease type 1A (CMT-TRIAAL and CMT-TRAUK): A double-blind randomised trial. *Lancet Neurology*, 10(4), 320–328. [https://doi.org/10.1016/S1474-4422\(11\)70025-4](https://doi.org/10.1016/S1474-4422(11)70025-4)
- Pestronk, A., & Drachman, D. B. (1978). A new stain for quantitative measurement of sprouting at neuromuscular junctions. *Muscle & Nerve*, 1(1), 70–74. <https://doi.org/10.1002/mus.880010110>
- Pipis, M., Rossor, A. M., Laura, M., & Reilly, M. M. (2019). Next-generation sequencing in Charcot-Marie-Tooth disease: Opportunities and challenges. *Nature Reviews. Neurology*, 15(11), 644–656. <https://doi.org/10.1038/s41582-019-0254-5>
- Preston, D. C., & Shapiro, B. E. (2013). *Electromyography and neuromuscular disorders: clinical-electrophysiologic correlations* (3rd ed.). Philadelphia, PA: Elsevier Saunders. Retrieved from <https://www.sciencedirect.com/book/9781455726721/electromyography-and-neuromuscular-disorders>
- Prukop, T., Stenzel, J., Wernick, S., Kungl, T., Mroczek, M., Adam, J., ... Sereda, M. W. (2019). Early short-term PXT3003 combination therapy delays disease onset in a transgenic rat model

- of Charcot-Marie-Tooth disease 1A (CMT1A). *PLoS One*, 14(1), e0209752. <https://doi.org/10.1371/journal.pone.0209752>
- Raeymaekers, P., Timmerman, V., Nelis, E., Jonghe, P. D., Hoogendijk, J. E., Baas, F., ... Bolhuis, P. A. (1991). Duplication in chromosome 17p11.2 in Charcot-Marie-Tooth neuropathy type 1a (CMT 1a). The HMSN Collaborative Research Group. *Neuromuscular Disorders*, 1(2), 93–97.
- Rossor, A. M., Evans, M. R. B., & Reilly, M. M. (2015). A practical approach to the genetic neuropathies. *Practical Neurology*, 15(3), 187–198. <https://doi.org/10.1136/practneurol-2015-001095>
- Rossor, A. M., Tomaselli, P. J., & Reilly, M. M. (2016). Recent advances in the genetic neuropathies. *Current Opinion in Neurology*, 29(5), 537–548. <https://doi.org/10.1097/WCO.0000000000000373>
- Roy, S., & Bhat, R. (2018). Effect of polyols on the structure and aggregation of recombinant human γ -Synuclein, an intrinsically disordered protein. *Biochimica et Biophysica Acta (BBA)—Proteins and Proteomics*, 1866(10), 1029–1042. <https://doi.org/10.1016/j.bbapap.2018.07.003>
- Schäfer, R., & Wernig, A. (1998). Polyclonal antibodies against NCAM reduce paralysis-induced axonal sprouting. *Journal of Neurocytology*, 27(8), 615–624.
- Schlebach, J. P., Narayan, M., Alford, C., Mittendorf, K. F., Carter, B. D., Li, J., & Sanders, C. R. (2015). Conformational stability and pathogenic misfolding of the integral membrane protein PMP22. *Journal of the American Chemical Society*, 137(27), 8758–8768. <https://doi.org/10.1021/jacs.5b03743>
- Scicchitano, B. M., Rizzuto, E., & Musarò, A. (2009). Counteracting muscle wasting in aging and neuromuscular diseases: The critical role of IGF-1. *Aging*, 1(5), 451–457. <https://doi.org/10.18632/aging.100050>
- Scurry, A. N., Heredia, D. J., Feng, C.-Y., Gephart, G. B., Hennig, G. W., & Gould, T. W. (2016). Structural and functional abnormalities of the neuromuscular junction in the Trembler-J homozygote mouse model of congenital hypomyelinating neuropathy. *Journal of Neuropathology and Experimental Neurology*, 75(4), 334–346. <https://doi.org/10.1093/jnen/nlw004>
- Sereda, M., Griffiths, I., Pühlhofer, A., Stewart, H., Rossner, M. J., Zimmermann, F., ... Nave, K.-A. (1996). A transgenic rat model of Charcot-Marie-Tooth disease. *Neuron*, 16(5), 1049–1060. [https://doi.org/10.1016/S0896-6273\(00\)80128-2](https://doi.org/10.1016/S0896-6273(00)80128-2)
- Sereda, M. W., Meyer zu Hörste, G., Suter, U., Uzma, N., & Nave, K.-A. (2003). Therapeutic administration of progesterone antagonist in a model of Charcot-Marie-Tooth disease (CMT-1A). *Nature Medicine*, 9(12), 1533–1537. <https://doi.org/10.1038/nm957>
- Shi, L., Fu, A. K. Y., & Ip, N. Y. (2012). Molecular mechanisms underlying maturation and maintenance of the vertebrate neuromuscular junction. *Trends in Neurosciences*, 35(7), 441–453. <https://doi.org/10.1016/j.tins.2012.04.005>
- Sociali, G., Visigalli, D., Prukop, T., Cervellini, I., Mannino, E., Venturi, C., ... Schenone, A. (2016). Tolerability and efficacy study of P2X7 inhibition in experimental Charcot-Marie-Tooth type 1A (CMT1A) neuropathy. *Neurobiology of Disease*, 95, 145–157. <https://doi.org/10.1016/j.nbd.2016.07.017>
- Spaulding, E. L., Sleight, J. N., Morelli, K. H., Pinter, M. J., Burgess, R. W., & Seburn, K. L. (2016). Synaptic deficits at neuromuscular junctions in two mouse models of Charcot-Marie-Tooth type 2d. *Journal of Neuroscience*, 36(11), 3254–3267. <https://doi.org/10.1523/JNEUROSCI.1762-15.2016>
- Uncini, A., & Kuwabara, S. (2015). Nodopathies of the peripheral nerve: An emerging concept. *Journal of Neurology, Neurosurgery, and Psychiatry*, 86(11), 1186–1195. <https://doi.org/10.1136/jnnp-2014-310097>
- Van Dijk, J. G., Van Bente, I., Kramer, C. G., & Stegeman, D. F. (1999). CMAP amplitude cartography of muscles innervated by the median, ulnar, peroneal, and tibial nerves. *Muscle & Nerve*, 22(3), 378–389. [https://doi.org/10.1002/\(SICI\)1097-4598\(199903\)22:3<378::AID-MUS11>3.0.CO;2-2](https://doi.org/10.1002/(SICI)1097-4598(199903)22:3<378::AID-MUS11>3.0.CO;2-2)
- Vita, G., Vita, G. L., Stancanelli, C., Gentile, L., Russo, M., & Mazzeo, A. (2019). Genetic neuromuscular disorders: Living the era of a therapeutic revolution. Part 1: peripheral neuropathies. *Neurological Sciences*, 40(4), 661–669. <https://doi.org/10.1007/s10072-019-03778-7>
- Wang, H.-Y., & Burns, L. H. (2009). Naloxone's pentapeptide binding site on filamin A blocks mu opioid receptor-Gs coupling and CREB activation of acute morphine. *PLoS One*, 4(1), e4282. <https://doi.org/10.1371/journal.pone.0004282>
- Wang, H.-Y., Frankfurt, M., & Burns, L. H. (2008). High-affinity naloxone binding to filamin A prevents mu opioid receptor-Gs coupling underlying opioid tolerance and dependence. *PLoS One*, 3(2), e1554. <https://doi.org/10.1371/journal.pone.0001554>
- Zhao, H. T., Damle, S., Ikeda-Lee, K., Kuntz, S., Li, J., Mohan, A., ... Kordasiewicz, H. B. (2018). PMP22 antisense oligonucleotides reverse Charcot-Marie-Tooth disease type 1A features in rodent models. *Journal of Clinical Investigation*, 128(1), 359–368. <https://doi.org/10.1172/JCI96499>

SUPPORTING INFORMATION

Additional supporting information may be found online in the Supporting Information section.

Figure S1. Supporting behavioral performances for increasing dosages of PXT3003 in CMT1A rats. Balanced stratification was achieved prior to therapy start in 4 weeks aged CMT1A rats for grip strength hindlimbs (a) and inclined plane behavior (b). Supplementary analyses of grip strength hindlimbs (raw data; c) and bar holding time (change from baseline; d) at study end. Inclined plane behavior throughout the entire study period (e) in CMT1A rats treated with increasing dosages of PXT3003 and at study end (f). (g) Two-way ANOVA results on transformed data as change from baseline: F_{Time} (1.429, 135.8) = 17.22; $p < 0.0001$; F_{Group} (4,95) = 0.5144 $p = 0.7253$; $F_{\text{Time} \times \text{Group}}$ (8, 190) = 0.3881 $p = 0.9261$. No body weights effects were observed for PXT3003 in CMT1A rats at study end (h). $n = 19$ –21 per group. a, b, c, e, f and h; t test. d and g; two-way ANOVA + Dunnett. $^{\#}p < 0.05$ CMT1A placebo vs. WT placebo; $^{*}p < 0.05$ CMT1A PXT3003 versus CMT1A placebo; dot plots and means, otherwise means and SD (e)

Figure S2. Supporting behavioral performance for dual combinations compared to PXT3003-3 in CMT1A rats. Balanced stratification was achieved prior to therapy start in 4 weeks aged CMT1A rats for grip strength hindlimbs (a) and inclined plane behavior (b). Supplementary analyses of grip strength hindlimbs (c) and bar holding time (d) at study end. Inclined plane behavior throughout the entire study period (e) in CMT1A rats treated with dual combinations of PXT3003-3 and at study end (f). (g) Two-way ANOVA results on transformed data as change from baseline: F_{Time} (1.819, 171.0) = 1.774 $p = 0.1759$, F_{group} (4, 94) = 2.881, $p = 0.0267$; $F_{\text{Time} \times \text{Group}}$ (8, 188) = 1.461, $p = 0.1739$. No body weights effects were observed for dual combinations of PXT3003-3 in CMT1A rats at study end (h). $n = 19$ –21 per group. a, b, c, d, e, f and h; t test. g; two-way ANOVA + Dunnett. $^{\#}p < 0.05$ CMT1A placebo versus WT placebo; $^{*}p < 0.05$ CMT1A any treatment versus CMT1A placebo; $^{*}p < 0.05$ CMT1A PXT3003-3 versus CMT1A dual combinations; dot plots and means, otherwise means and SD (E)

Figure S3. Supporting electrophysiological, molecular, and muscle data in CMT1A rats. In the sciatic nerve, no therapy effects were observed for PXT3003-3 and its dual combinations on motor latency after distal stimulation (a), NCV (b) and distal CMAP electrophysiological recordings (c). Transcriptional and histological analyses revealed lacking therapy effects for PXT3003-3 and its dual combinations on *Pmp22* (d) and *Sox2* (e) mRNA expression, and on the number of myelinated axons (f). Type IIb specific mRNA expression was in line with immunohistological effects in CMT1A rats treated with PXT3003-3 (g). $n = 5\text{--}20$ per group; t tests; $^{\#}p < 0.05$ CMT1A placebo versus WT placebo; dot plots and means

Transparent Science Questionnaire for Authors

Transparent Peer Review Report

How to cite this article: Prukop T, Wernick S, Boussicault L, et al. Synergistic PXT3003 therapy uncouples neuromuscular function from dysmyelination in male Charcot-Marie-Tooth disease type 1A (CMT1A) rats. *J Neurosci Res.* 2020;00:1–20. <https://doi.org/10.1002/jnr.24679>